2012

Lattice Boltzmann Applied to Fluid Flow and Heated Lid-Driven Using 2D Square Lattice Dimension (D2Q9)

Saeed J. Almalowi
Lehigh University

LATTICE BOLTZMANN APPLIED TO FLUID FLOW AND HEATED LID-DRIVEN USING 2D SQUARE LATTICE DIMENSION (D2Q9)

By

(SAEED J. ALMALOWI)

A Thesis
Presented to the Graduate and Research Committee
of Lehigh University
in Candidacy for the Degree of
(Master of Science)

In

(DEPARTMENT OF MECHANICAL ENGINEERING AND MECHANICS)

Lehigh University

2012

Thesis is accepted and approved in partial fulfillment of the requirements for the Master of Science in Mechanical Engineering Department

LATTICE BOLTZMANN APPLIED TO FLUID FLOW AND HEATED LID-DRIVEN USING 2D LATTICE DIMENSION

SAEED J. ALMALOWI

Date Approved

PROF. Alparslan OZTEKIN
Advisor

PROF. Gary D. Harlow
Department Chair Person

Abstract

Lattice Boltzmann method is implemented to study 2D hydrodynamically and thermally developing steady laminar flows in a channel and the lid-driven cavity flows. Numerical simulation of two dimensional convective heat transfer problem is conducted using nine directional D2Q9 thermal lattice Boltzmann arrangements. The velocity and temperature profiles in the developing region predicted by Lattice Boltzmann method are compared against those obtained by ANSYS-FLUENT. Velocity and temperature profiles as well as the skin friction and the Nusselt numbers agree very well with those predicted by the self similar solutions of fully developed flows. Furthermore, simulations of velocity and temperature filed in 2D lid-driven cavity flows are conducted by using D2Q9 thermal lattice Boltzmann technique. The velocity and temperature profiles predicted by velocity and temperature profiles predicted by LBM agree well with those obtained by ANSY-FLUENT. It is clearly shown here that thermal lattice Boltzmann method is an effective computational fluid dynamics (CFD) tool to study nonisothermal flow problems.

Nomenclatures

f	Density distribution function
f^{eq}	Local equilibrium density distribution function
g	Temperature distribution function
g^{eq}	Local equilibrium temperature distribution function
$\mathbf{c}=(c_x,c_y)$	Lattice discrete velocity, c_x and c_y are x- and y-components
$\mathbf{V}=(u,v)$	Bulk velocity of the fluid, u and v are x- and y-components
U	Normalized x-component of the fluid velocity
θ	Normalized temperature
ω	Dimensionless relaxation frequency
w	Weight factor
T_w	Wall temperature in (°C)
c_s	Lattice sound speed
τ	Dimensionless collision relaxation time
$\mathbf{r}$	Position vector
(X,Y)	Dimensionless x and y coordinate
U_{in}	Fluid speed at the inlet
T_{in}	Temperature profile at the inlet in (°C), $T_{in}(y)$
ρ	Density of fluid, kg/m^3
υ	Kinematic viscosity of fluid, m^2/sec
α	Thermal diffusivity of fluid, m^2/sec
Pr	Prandtl Number
Re	Reynolds Number
T	Bulk temperature in (°C)

ACKNOWLEDGEMENTS

I would like to thank all my friends, colleagues and teachers especially my supervisor, extended their whole hearted cooperation for the completion of this task.

I would like to acknowledge the valuable guidance of my supervisor Professor Oztekin who at every step of my research work assisted me. Prof. Oztekin is the person who helped me and gave me so many suggestions for my research work. I would like to thank him for his patience and device.

I would like to appreciate Taibah University in KSA for giving me scholarship and supported me to complete my study overseas. Moreover, I'll extend my acknowledgement to Saudi Arabia government for financial support.

I am thankful to all the professors who taught me during my study for Master degree at Lehigh University. I gained so many benefits from them since I attended to Lehigh School in 2010. I really appreciated all of them.

I am greatly appreciative of the friendship with my friends, especially Hoalin and Ali for his help with ANSYS-FLUENT.

Back home, I wish to thank my parents, brothers, and sisters for their help and encouragement to complete this work. I would like to give a very special thanks to Dr. Yasir Al-sharif, Professor of Mechanical Engineering at Taibah University, Almadinah, Saudi Arabia, for his guidance and encouragement and for his unlimited advice and suggestions in my academic life.

Finally, I really thank my wife and my son for their great sacrifices and endless support they provided during my study in the United States. Thanks for their patience during the times I was occupied with this work. For them, I owe a lot.

TABLE OF CONTENETS **PAGE**

LIST OF ILLUSTRATIONS

FIGURE **PAGE**

LIST OF TABLES

TABLE **PAGE**

CHAPTER 1: INTRODUCTION, MOTIVATION A ND LITERATURE REVIEW

Introduction

Ludwig Eduard Boltzmann (1844-1906), the Austrian physicist, had the greatest achievement in the development of statistical mechanics. This approach has been used to predict macroscopic properties of matter such as the viscosity, thermal conductivity, and diffusion coefficient from the microscopic properties of atoms and molecules [1-3]. The probability of finding particles within certain range of velocities at a certain range of locations replaces tagging each particle as in molecular dynamic simulation. Historically, the lattice Boltzmann method originated from the lattice-gas cellular automata method (LGCA)[4], The LBGK which is known as the lattice Bhatnagar-Gross-Krook method has been developed rapidly and applied for many studies. The nonlinear term in the lattice Boltzmann approximated by BGK to become linear term, and this term is known as the collision term in the lattice BGK governing equation. The main idea of LBM is to bridge the gap between micro-scale and macro-scale by not considering individual behavior of particles alone but behavior of a collection of particles as a unit. The property of particle is represented by a distribution function. The distribution function acts as a representative for collection of particles. This scale is unknown as mesoscopic scale. The terminology of the kinetic theory is the heart of lattice Boltzmann equation. The thesis is outlined as follows: The lattice Boltzmann governing equation and its arrangements, LBM mode, and BCs are discussed in chapter2. The results are presented in chapter 3 for thermally developing flow using D2Q square lattice. The results for nonisothermal cavity flow are presented in chapter 4 using D2Q9 thermal lattice Boltzmann method. Conclusion and future work are presented in chapter 5.

1.1 MOTIVATION

Since its precursor-the lattice gas automaton (LGA) was proposed more than twenty years ago as a useful computational fluid dynamics (CFD) method. The lattice Boltzmann method has emerged as promising approach for simulation either simple flow or complex flow. Although the lattice Boltzmann is more advanced simulation method, the researchers focused more on the traditional simulation technique. The lattice Boltzmann is used to solve microscopic or mesoscopic kinetic equations. It is unlike traditional (CFD) method which solves macroscopic equations by solving Navier stokes equation. The beauty of LBM in treating multi-phase flows -for instance- is that there is no need to trace the interface between phases as in the case of NSE. Moreover, the attractive advantages of LBM is that it can be naturally adapted to parallel processes computing, there is no need to solve Laplace equation at each time step to satisfy the continuity equation of incompressible flow as it is in solving Navier-Stokes equation (NSE). However, LBM needs more computer memory compared with NS E solver, which is not a huge constraint.

Furthermore, LBM can be used to handle a problem in micro-and macros-scales with reliable accuracy. Our motivation is that we would like to apply LBM not only for two dimensional single flows, but also would like to model multi-phase-three dimensional flows using LBM method. Study complex flows will be difficult to be solved using traditional (CFD) technique. Researchers have used LBM to solve single and multi-phase flows [5,6]. As we conclude that LBM is a promising simulation tool for not only complex computational flow simulation.

1.2 LITERATURE REVIEW

Many approaches of the lattice Boltzmann scheme have been discussed [Skordos (1993), Nobel; Chen Shan, and Mei (1996)]. However, a successful LBM simulation rests on the correct implementation of the boundary conditions, where unknown distribution functions originated from the operation. As it stated in several literature, the implementation of the boundary conditions in the LBM is a challenging task. In this work, the lack of accuracy caused by less accurate discrete of boundary condition with the conservation of mass and momentum at each BCs is avoided.

Furthermore, pervious investigators applied hydrodynamically developing flow in channels for low Reynolds numbers (Re=2,10,12) [7,8]. One of the this work is to apply LBM for hydromdynamicall and thermally developing flow at high Reynolds number. Nonisothermal steady 2D cavity flow will also be studied at Re=1000, Re=5000, and Re=10000 and the results of LBM method will be compared against those obtained by Fluent.

Qisu Zou et al 1996 used velocity flow boundary conditions and bounce back for the lattice Boltzmann BGK model (D2Q9) at Re=10 with single relaxation time which is different for different value of Re. He presented unstable results for certain type of BCs [7]. Lattice Boltzmann D2Q9 was implemented for simulating thermal flow in compressible fluids by Bruce J. Plamer et al 1999 for Pr=1 & 2 and Re=200 [8]. A thermal lattice Boltzmann was applied by X.D. Niu et al 2005 with diffuse scattering boundary condition for micro thermal flows [8]. LBM D2Q9 model was applied for fluid-fluid conjugate heat transfer by Jinku Wang et al 2006. They studied and compared some results with the analytical solution [9].

Ghia et al (1982) employed stream function-vorticity method to solve NSE. They used implicit multi-grid method to two dimensional lid-driven cavity flow at various Reynolds numbers (Re=100,400,5000,and 10000) [10]. Renwei Mei et al 2002 used LBM to study lid-driven cavity flow for Rynolds number (Re=100,400,100, and 2000) with uniform grids [7]. E. Erturk et al 2003 using NSE multi-grid method to investigate the 2D lid-driven for Re up to 21000 [11].

LBM is implemented here to study thermally and hydrodynamically developing flow in channel and nonisothermal cavity flows. For these two problems, we compared our results against the results obtained by ANSYS-FLUENT and with some well documented results in the literature such as U.Ghia (1982) and E. Erturk et(2003) for squared lid-driven cavity flow.

CHAPTER 2: LATTICE BOLTZMMANN ARRANGMENTS AND BOUNDARY CONDITIONS

2.1. LATTICE BOLTZMANN GOVERNING EQUATION

The probability of finding particles within certain range of velocities at a certain range of locations replaces tagging each particle as in molecular dynamics simulation. The lattice Boltzmann transportation can be governed by distribution function which represents particles at location **r**(*x*,*y*) at time *t*, the particle will be displaced by (Δx,Δy) in time Δt with the application force F on the liquid molecules [11]. The equation governing the distribution function *f(x,y,***c**,*t)* has two terms, the streaming step and the collision term. Here *x* and *y* are spatial coordinates, *t* is the time and *c* is the lattice discrete velocity.

The collision takes place between the molecules; there will be a net difference between the numbers of molecules in the interval $drdc$. The rate of change of the distribution function is expressed as

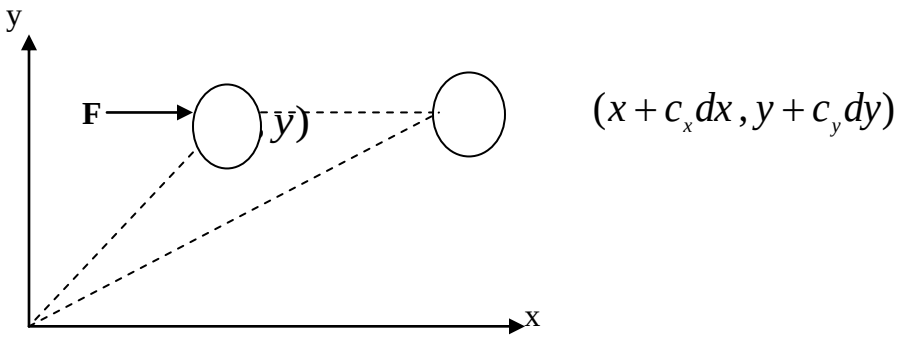

Figure 1. Kinetic Motion of Molecules

Here: $c_x = \frac{dx}{dt}, c_y = \frac{dy}{dt}$

With the collision takes place between the molecules, there will be a net difference between the numbers of molecules in the interval dxdydc. The collision terms is defined as the rate of change between final and initial status of the distribution function. Therefore, governing the distribution function is given by the equation (2.1):

$$f_i(x+dx, y+dy, Fdt/m, t+dt)dxdydc - f_i(x, y, c, t)dxdydc = \varphi(f_i)dxdydcdt \quad (2.1)$$

Dividing both side of equation (2.1) by dxdydc yields:

$$\frac{f_i(\mathrm{x}+d\mathrm{x}, y+dy, c+\mathrm{F}dt/m, t+dt) - f_i(\mathrm{x}, \mathrm{y}, \mathrm{c}, t)}{dt} = \varphi(f_i) \quad (2.2)$$

With position vector: $\mathrm{r} = \mathrm{xi} + \mathrm{yj}$, the equation (2.2) can be written as

$$\frac{f_i(\mathrm{r}+d\mathrm{r}, c+\mathrm{F}dt/m, t+dt) - f_i(\mathrm{r}, \mathrm{c}, t)}{dt} = \frac{\partial f_i}{\partial t} + c_x\frac{\partial f_i}{\partial x} + c_y\frac{\partial f_i}{\partial y} + \frac{\mathrm{F}}{m}.\frac{\partial f_i}{\partial c} = \varphi(f_i) \quad (2.3)$$

Here *F* denotes external forces applied and *φ(f)* is the source or the collision term. With the absence of the external forces equation (2.1) becomes

$$\frac{\partial f_i}{\partial t} + c\cdot\nabla f_i = \varphi(f_i) \quad (2.4)$$

Equation (2.5) is known as the lattice Boltzmann governing equation. The right hand side of equation is called a source and is approximated by BGK as

$$\varphi(f_i) = \frac{1}{\tau}(f_i^{eq} - f_i)$$

Here $\omega = 1/\tau$ is the relaxation frequency and the τ is the relaxation time f^{eq} is the equilibrium value of distribution function and is written as

$$f_i^{eq} = w_i\rho\left[1 + \frac{3c_i\cdot\mathrm{V}}{c_s^{\,2}} + 4.5\frac{(c_i\cdot\mathrm{V})^2}{c_s^{\,4}} - 1.5\frac{\mathrm{V}\cdot\mathrm{V}}{c_s^{\,2}}\right] \quad (2.5)$$

where c_i is the discrete velocities vector, *V* is the bulk fluid velocity and w_i is the weight factor.

The equation (2.2) becomes

$$f_i(\mathrm{r}+\Delta\mathrm{r}, t+\Delta t) = (1-\omega)f_i(r,t) + \omega f_i^{eq} \quad (2.6)$$

2. 2. MODELING OF LATTICE BOLTZAMANN

2. 2.1. Momentum Lattice Boltzmann Model

The momentum LBM models of lattices [12]. For instance, in D2Q9 model, the lattice at the origin is at rest and the remaining lattices move in different directions with different speed. Each velocity vector is a lattice per unit step. These velocities are exceptionally convenient in that all x and y-components are either 0 or ±1. Mass of particle is taken as unity uniformly throughout the flow domain. The bulk fluid density is governed by conservation of mass

$$\rho = \sum_{i=1}^{9} f_i \tag{2.7}$$

The bulk fluid velocity (V = (u,v)) is the average of microscopic lattice directional velocities (c=(c_x,c_y)) and the directional densities and is governed by conservation of momentum

$$\mathrm{V} = \frac{1}{\rho}\sum_{i=1}^{9} f_i c_i \tag{2.8}$$

Here $c_x = dx/dt$, $c_y = dy/dt$ are x- and y-components of the lattice directional velocity. Conservation of mass and momentum are also applied at each boundary condition.

The kinematic viscosity is defined as $\upsilon = \frac{(\Delta x)^2}{3\Delta t}(\frac{1}{\omega} - \frac{1}{2})$ (2.9)

.2.2.2. Thermal Lattice Boltzmann Model

Recently, there has been rapid progress in developing the construction of stable thermal lattice Boltzmann equation models to study heat transfer problems. McNamara and Alder successfully applied multispeed thermal fluid lattice Boltzmann method to solve heat transfer problems [6]. At the outlet, bounce back or extrapolation boundary conditions are considered as the thermal and flow boundary conditions. Bounce back type boundary conditions are proven to provide more accurate numerical approximations [11] and are used by the present work. The temperature at each wall is specified. The temperatures which are pointing to the flow domain are unknowns and they can be evaluated from streaming and collision steps.

For the thermal distribution function, the equation (2.4) can be written as

$$g_i(r + \Delta r, t + \Delta t) = (1 - \omega)g_i(r, t) + \omega g_i^{\ eq} \tag{2.10}$$

where g^{eq} as follow:

$$g_i^{eq} = \omega_i \theta \left[1 + \frac{3c_i \cdot \mathrm{V}}{c_s^2} + 4.5 \frac{(c_i \mathrm{V})^2}{c_s^4} - 1.5 \frac{\mathrm{V}.\mathrm{V}}{c_s^2} \right] \quad (2.11)$$

The normalized bulk fluid temperature is given by

$$\theta = \frac{T - T_w}{T_{in} - T_w} \quad (2.12)$$

The conservation of energy is given by

$$T = \sum_{i=1}^{9} \mathrm{g_i} \quad (2.13)$$

The thermal diffusivity is defined as $\alpha = \frac{(\Delta x)^2}{3\Delta t}(\frac{1}{\omega} - \frac{1}{2})$ (2.14)

2.3. LATTICE BOLTZAMMAN D2Q9 ARRANGMENT

2.3.1. Lattice Boltzmann Arrangements (D2Q9)

Lattice Boltzmann is relatively recent technique that has been shown to be as accurate as traditional CFD methods having ability to integrate arbitrarily complex geometrics. LBM can be used for different arrangements such as D1Q2, D2Q4, D2Q9, D3Q15, D3Q19, or D3Q27 [13]. In the present work, D2Q9 lattice will be used to examine noisothermal 2D problems. D2Q9 lattice arrangement is shown in figure 2.

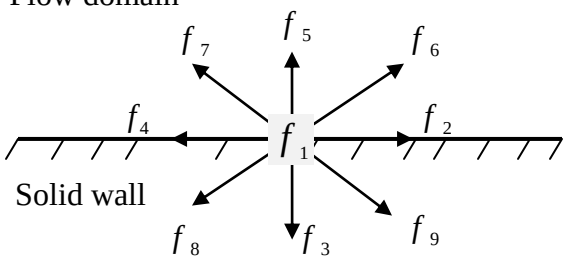

Figure 2. D2Q9 LBM

Each distribution function has position vector (*r*), velocity vector (*c*) and weight factor (*w*).

For D2Q9, the lattice veolcties and weight factor are given by

$$c_i = \begin{cases} (0,0) & i=1 \\ c([\sin(i\text{-}1)\pi/2],[\cos(i\text{-}1)\pi/2]) & i=2,3,4,5 \\ c(\sqrt{2}[\cos(2i\text{-}11)\pi/4],\sqrt{2}[\sin(2i\text{-}11)\pi/4]) & i=6,7,8,9 \end{cases} \quad (2.15))$$

$$w_i = \begin{cases} 4/9 & i=1 \\ 1/36 & i=6,7,8,9 \\ 1/9 & i=2,3,4,5 \end{cases} \quad (2.16)$$

2.4. BOUNDARY CONDITIONS

Applying boundary condition is the crucial part using LB method. There are several types of BCs which can be applied using LBM. First type is the first order bounce back boundary condition which is applied at the boundary. The second order bounce back BCs which is applied the half away from the boundary. Third type is applying conservation of mass and momentum at each boundary. In this section the type of boundary conditions imposed on both velocity and temperature filed will be discussed.

2.4.1. FIRST ORDER AND SECOND ORDER BOUNCE BACK

2.4.1.1. First Order Bounce Back

This type of the boundary condition determines the unknown distribution functions at the boundary with the first order of accuracy as so many researchers claimed. It doesn't give accurate results for developing flow inside the channel. The schematic diagram shown below illustrates the first order bounce back type of boundary condition is applied.

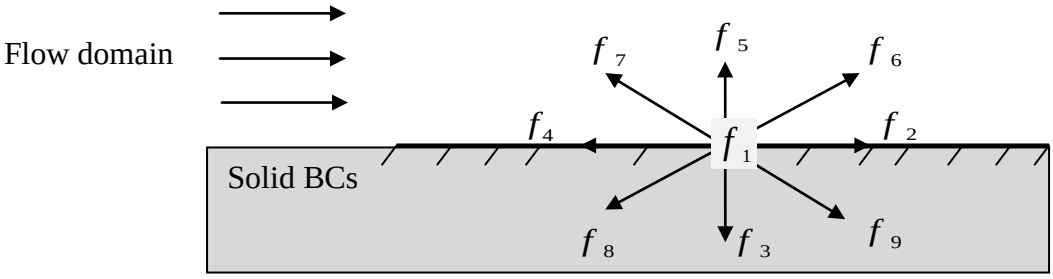

Figure 3. 1st order bounce back

Each distribution function reflects inside the flow domain as shown in figure3:

The unknown distribution functions are f_6 , f_5 , and f_7

$$f_6 = f_8,\ f_5 = f_3, \text{and } f_7 = f_9$$

The distribution functions f_8 , f_3 , and f_9 are known which can be evaluated from streaming step and collision step.

2.4.1.2. Second Order Bounce Back

In the second order bounce back, the distribution functions are located half way from the solid boundary. This type of boundary condition is known as the second order bounce back boundary condition. Application of the second order bounce back type of boundary condition provides more accurate results against those with the first order bounce back boundary condition. Figure 4 shows how this type of the boundary condition is applied.

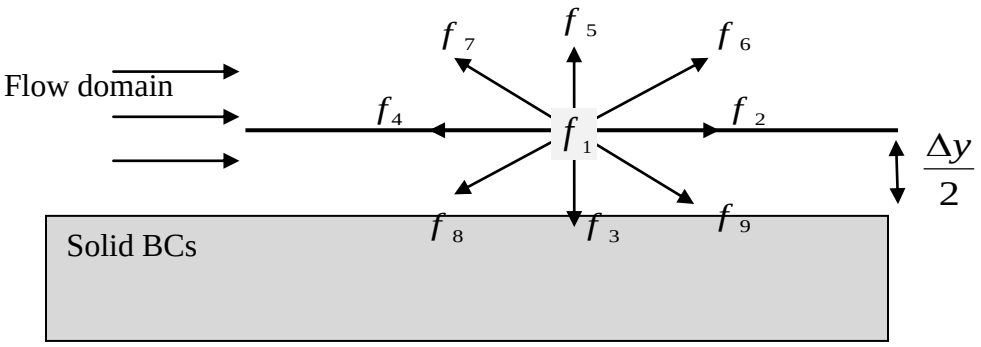

Figure 4. 2nd order bounce back

The unknown distribution functions are f_6 , f_5 , and f_7

$$f_6 = f_8,\ f_5 = f_3, \text{and } f_7 = f_9$$

The distribution functions are f_8 , f_3 , and f_9 are known which can be evaluated from streaming step and collision step. Notice that, the f_8 , f_3 , and f_9 are inside the flow domain and shifted away from the solid BCs by $\frac{\Delta y}{2}$.

2.4.2. NEUMMAN BOUNDARY CONDITIONS (VELOCITY KNOWN)

For this type of boundary conditions, the conservation of mass and conservation of momentum are applied at each boundary. For D2Q9, there are nine velocities components pointed in different directions.

Applying the conservation of mass yields:

$$\rho = \sum_{i=1}^{9} f_i = f_1 + f_2 + f_3 + f_4 + f_5 + f_6 + f_7 + f_8 + f_9 \qquad (2.17)$$

Applying the conservation of momentum yields:

$$\mathrm{u} = \frac{1}{\rho}(f_2 + f_6 + f_9 - f_7 - f_4 - f_8) \qquad (2.18)$$

$$\mathrm{v} = \frac{1}{\rho}(f_5 + f_6 + f_7 - f_3 - f_8 - f_9) \qquad (2.19)$$

Adding equations (2.18) and equation (2.19) yields:

$$\rho(\mathrm{u} + \mathrm{v}) = f_2 + f_5 + 2f_6 - f_4 - f_3 - 2f_8 \qquad (2.20)$$

Equations (2.17-2.20) have four unknowns; namely three distribution functions pointing inside the flow domain and the density.

Using the local equilibrium distribution function perpendicular to the boundary provides

$$f_5 - f_5^{eq} = f_3 - f_3^{eq} \Rightarrow f_3 = f_5 \qquad (2.21)$$

Here no-slip condition is applied at the upper and lower plates.

Substitution equation (2.21) into equation (2.20) yields:

$$\rho(\mathrm{u} + \mathrm{v}) = f_2 + 2f_6 - f_4 - 2f_8 \qquad (2.22)$$

In equation (2.15) there are two unknowns; namely f_6 and ρ

Substitution equation (2.14) into equation (2.10) and adding equation (2.10) to equation (2.11) yield to:

$$\rho(1 + \mathrm{u}) = f_1 + 2f_2 + 2f_5 + 2f_9 + 2f_6 \qquad (2.23)$$

Subtracting equation (2.15) from equation 2.16 yields:

$$\rho_u = \frac{f_1 + f_2 + f_4 + 2\times(f_3 + f_9 + f_8)}{1-v} \quad (2.24)$$

$$\rho_u = \frac{f_1 + f_2 + f_4 + 2\times(f_5 + f_7 + f_6)}{1+v} \quad (2.25)$$

$$f_3 = f_5 - \frac{2}{3}\rho_u \times v \quad (2.26)$$

$$f_8 = f_6 - \frac{1}{2}(f_4 - f_2)\frac{1}{2}\rho_u \times v - \frac{1}{2}\rho_u \times u \quad (2.27)$$

$$f_9 = f_7 + \frac{1}{2}(f_4 - f_2) - \frac{1}{6}\rho_u \times v + \frac{1}{2}\rho_u \times u \quad (2.28)$$

Similarly at the lower boundary no-slip and no penetration condition yields

$$\rho_u = \frac{f_1 + f_2 + f_5 + 2\times(f_3 + f_9 + f_8)}{1+v} \quad (2.29)$$

$$f_5 = f_3 + \frac{1}{2}\rho_l \times v \quad (2.30)$$

$$f_6 = f_8 + \frac{1}{2}(f_4 - f_2) + \frac{1}{6}\rho_l \times v + \frac{1}{2}\rho_l \times u \quad (2.30)$$

$$f_7 = f_9 - \frac{1}{2}(f_4 - f_2) + \frac{1}{6}\rho_l \times v - \frac{1}{2}\rho_l \times u \quad (2.31)$$

At the inlet:

$$f_4 - f_4^{eq} = f_2 - f_2^{eq} \quad (2.32)$$

$$\rho_{in} = \frac{f_1 + f_5 + f_3 + 2\times(f_4 + f_7 + f_8)}{1-u_{in}} \quad (2.33)$$

$$f_2 = f_4 + \frac{2}{3}\rho_{in} \times u_{in} \quad (2.34)$$

$$f_9 = f_8 + \frac{1}{6}\rho_{in} \times u_{in} \quad (2.35)$$

$$f_5 = f_7 + \frac{1}{6}\rho_{in} \times u_{in} \quad (2.36)$$

For the outlet condition (account for an open BCs)

The outlet boundary condition can be taken outflow boundary condition, by using second order extrapolation which yields

$$f_2(N) = 2f_2(N-1) - f_2(N-2) \quad (2.31)$$

$$f_6(N) = f_6(N-1) - f_6(N-2) \quad (2.32)$$

$$f_9(N) = f_9(N-1) - f_9(N-2) \quad (2.33)$$

Where N is the number of lattice nodes in x-direction. If the outlet velocity is known, the conservation of mass and conservation of momentum can be applied at the outlet to determine distribution functions.

2.4.3. Thermal Boundary Conditions

Various types of thermal boundary conditions will be discussed here for D2Q9 thermal lattice Boltzmann arrangements. These boundary conditions are adiabatic, constant heat flux, and constant temperature at the boundary. Several investigators have studied some of these type of thermal boundary condition.

2.4.3.1. Adiabatic Boundary Condition

When the upper and lower boundary are insulated (no heat moves over the boundary), the heat flux " q " should be equal zero. The boundary conditions for both surfaces (Upper and Lower surface) become:

$$k\frac{\partial T}{\partial y} = k\frac{T(j+1,i) - T(j,i)}{\Delta y} = 0 \quad (2.34)$$

$$k\frac{g_k(j+1,i) - g_k(j,i)}{\Delta y} = 0 \rightarrow g_k(j+1,i) - g_k(j,i) = 0 \quad (2.35)$$

$$g_k(1,i) = g_k(2,i) \tag{2.36}$$

$$g_k(n,i) = g_k(n-1,i) \tag{2.37}$$

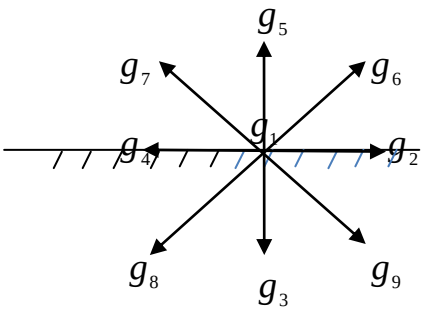

Figure 5. D2Q9 Thermal distribution functions

2.2.2. Constant Temperature at the Upper and theLower Boundary

$$T_W = \sum_{k=1}^{9} g_k = g_1 + g_2 + g_3 + g_4 + g_5 + g_6 + g_7 + g_8 + g_9 \text{ or} \tag{2.38}$$

$$\theta_W = \sum_{k=1}^{9} g_k = g_1 + g_2 + g_3 + g_4 + g_5 + g_6 + g_7 + g_8 + g_9 \tag{2.39}$$

In case of the temperature is constant (T=Tw) at the lower and upper boundary condition:

$$g_3(= \theta_w(w(5) + w(3)) - g_5 \tag{2.40}$$

$$g_8 = \theta_w(w(6) + w(8)) - g_6 \tag{2.41}$$

$$g_9(= \theta_w(w(7) + w(9)) - g_7 \tag{2.42}$$

2.4.3.2. Constant Flux Boundary Condition

In case of the upper and lower boundary are at constant heat flux (There is a heat moves over the boundary), the heat flux “q " should be mentioned as it is defined in the Fourier law. The boundary conditions for both surfaces (Upper and Lower surface) become:

$$q = k\frac{\partial T}{\partial y} = k\frac{T(j+1,i) - T(j,i)}{\Delta y} \tag{2.43}$$

$$k\frac{g_k(j+1,i) - g_k(j,i)}{\Delta y} = q \rightarrow g_k(j+1,i) - g_k(j,i) = \frac{q\Delta y}{k} \tag{2.44}$$

In case of the heat flux is constant at the upper surface:

$$g_k(n,i) = g_k(n-1,i) - \frac{q\Delta y}{k} \tag{2.45}$$

In case of the heat flux is constant at the lower surface:

$$g_k(1,i) = g_k(2,i) - \frac{q\Delta y}{k} \tag{2.46}$$

The local and Average Nusselet Number

$$Nu = \frac{D_h h}{k_f},\ q = k_f \frac{\partial T}{\partial y}, \text{where } \mathrm{D_h} = 2H$$

$$q = h\ (T_s - T_m) = k_f \frac{\partial T}{\partial y} \tag{2.47}$$

The mean temperature can be evaluated by:

$$T_m = \frac{\int u_y T dA}{\int u_y dA} = \frac{\int u_y T dY}{\int u_y dY} \tag{2.48}$$

Where $\mathrm{T_s}$ is the surface temperature

The average Nusselt number is

$$\overline{Nu} = \int_0^1 Nu\ dX \tag{2.49}$$

$$\theta = \frac{T - T_{in}}{T_W - T_{in}}, \mathrm{Y} = \frac{\mathrm{y}}{\mathrm{H}}, \mathrm{X} = \frac{\mathrm{x}}{\mathrm{L}} \tag{2.50}$$

After applying the scaling yields:

$$q = k_f \frac{\partial T}{\partial y}, \quad h = \frac{\frac{k_f}{H}\frac{\partial \theta}{\partial Y}}{(T_S - T_m)},\ Nu = \frac{1}{(T_S - T_m)}\frac{\partial \theta}{\partial Y} \tag{2.51}$$

CHAPTER 3: STEADY STATE TWO DIMENSIONAL HYDRODYNAMICALLY THERMALLY DEVELOPING IN A CHANNEL

3.1. PROBELEM STSTAMENT

Hydrodynamically and thermally developing flow in the entrance region of a channel is considered. At the upper and the lower boundary no-slip and no penetration is applied. At the fluid velocity is uniform U=0.02m/sec. The height of channel is 0.02m and the aspect ratio is AR=50. The temperature is constant at the upper and the lower boundary and the temperature profile at the inlet is taken as $\theta_{in} = 4\times(Y - Y^2)$. Figure 6 displays the velocity, temperature boundary conditions and the inlet condition.

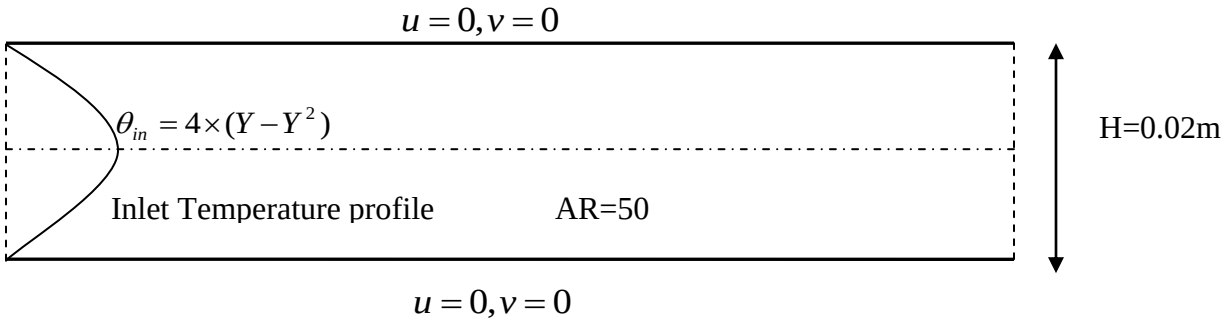

Figure 6. Flow Geometry

The scaling parameters are

$$\theta = \frac{T - T_{in}(H/2)}{T_W - T_{in}(H/2)}, \mathrm{Y} = \frac{\mathrm{y}}{\mathrm{H}}, \mathrm{X} = \frac{\mathrm{x}}{\mathrm{L}}$$

3.2. APPLYING LATTICE BOLTZMANN (D2Q9) TO HYDRODYNAMICALLY THERMALLY DEVELOPING

The conservation of mass is expressed as

$$\rho = \sum_{i=1}^{9} f_i$$

The bulk fluid velocity (V = (u,v)) is the average of microscopic lattice directional velocities (c=(c_x,c_y)) and the directional densities and is governed by conservation of momentum

$$\mathrm{V} = \frac{1}{\rho}\sum_{i=1}^{9} f_i c_i$$

Here $c_x = dx/dt$, $c_y = dy/dt$ are x- and y-components of the lattice directional velocity. Conservation of mass and momentum are also applied at each boundary as shown in figure7.

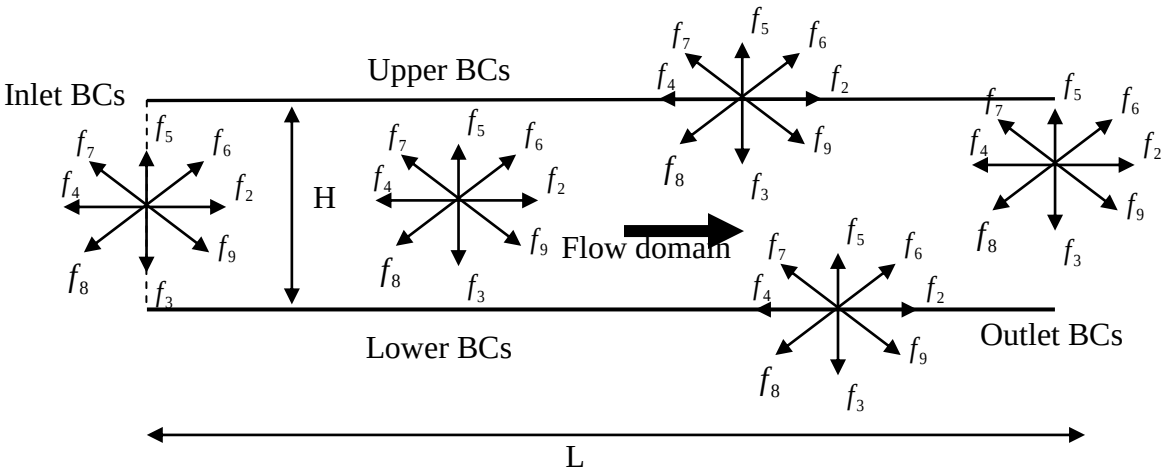

Figure 7. Velocity boundary conditions schematic diagram

The inlet velocity is U_{in} , the length of channel is L and the distance between lower and upper plate is H. u is measured in units of U_{in} ($U = u/U_{in}$), x and y are measured in units of L and H ($X = x/L$ and $Y = y/H$), respectively. Scaled inlet velocity becomes $U = 1$ and the flow domain (X,Y) becomes $0 \geq \mathrm{Y} \leq 1, \text{ and } 0 \leq \mathrm{X} \geq 1.$

The conservation of energy is expressed as

$$T = \sum_{i=1}^{9} g_i$$

The temperature at each wall is specified. The temperatures which are pointing to the flow domain are unknowns and they can be evaluated from streaming and collision steps as shown in the Figure 8.

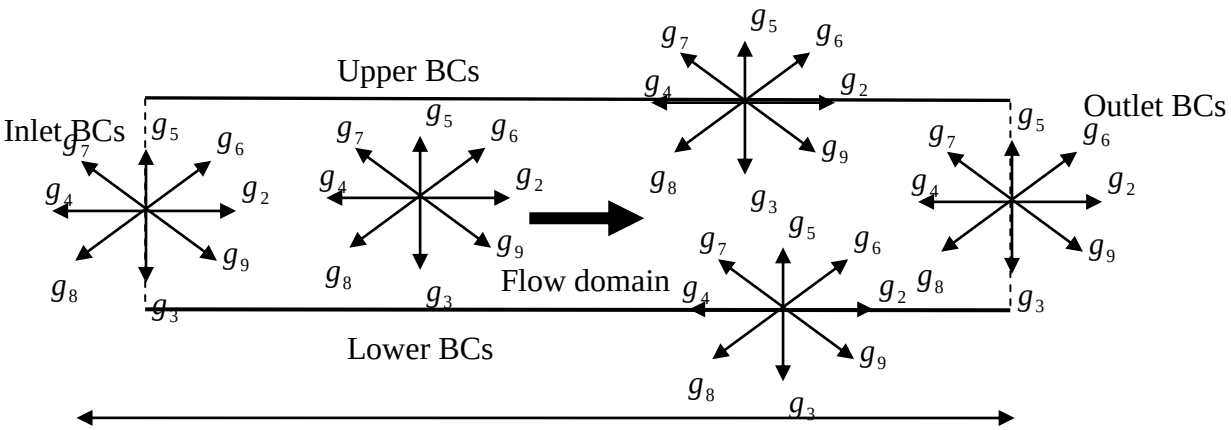

Figure.8. Temperature boundary conditions schematic diagram

3.3. Results and Discussion

The results are presented for steady incompressible two dimensional laminar flows in an entrance region of a channel. Flow develops hydrodynamically and thermally in a 1m long and 0.02m height channel with the aspect ratio AR of 50. At the inlet the flow is uniform ($U_{in} = 0.02m/\sec$) and the temperature of the fluid satisfies $\theta_{in} = 4\times(Y - Y^2)$. Boundary conditions imposed on the velocity field at Y = 0 and 1 are no-slip and no-penetration and the thermal boundary conditions applied on each surface is θ = 0. The physical properties are considered to be constant and are determined for water at 300K - ($\rho = 999.1kg/m^3$ and $\mu = 855\times10^{-3} N.s/m^2$). For the example illustrated in this paper the flow rate considered is 0.4 kg/s and the corresponding Reynolds number $Re = \rho 2HU_{in}/\mu$ = 800[18].

Spectral convergence is checked for LBM to ensure that the results predicted by the LBM are not dependent on the number of nodes selected for the numerical simulations. Nodes (*N*x*M*) are placed uniformly in the direction of x (*N* nodes) and y (*M* nodes). The convergence test is displayed in Figure 9 as the velocity and temperature profile at X = 0.2 plotted for various *N* and *M*. It is shown that the (50×1000) mesh provides satisfactory spectral convergence and numerical accuracy and is thereby chosen for the numerical simulation results predicted by LBM.

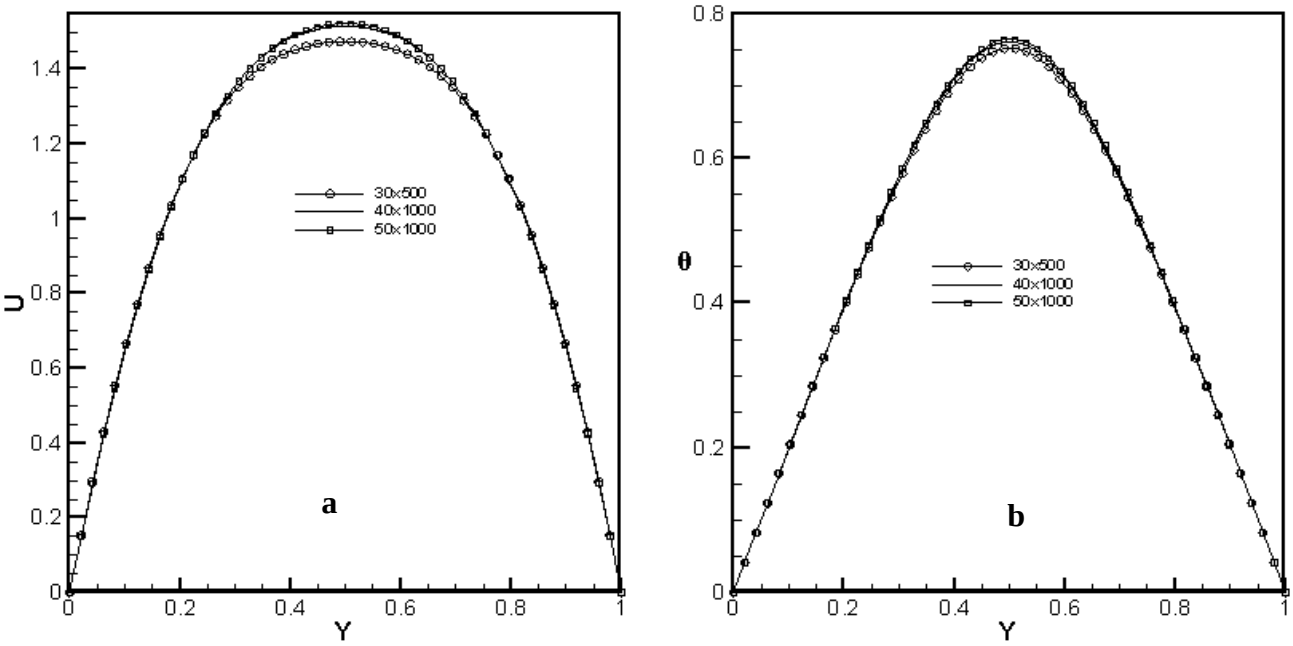

Figure 9. a) Velocity and b) temperature profiles at X=0.2 plotted for various N and M

The velocity and temperature profiles are displayed at various cross-sections in the developing region. The profiles that are obtained by LBM are compared against those obtained by ANSYS-FLUENT at the same conditions. The boundary conditions at the inlet and the outlet and on the surface of the plates are selected as the same for both methods. The Gauss-Siedel iterative method has been employed for LBM simulations.

The velocity and temperature field are considered to be converged when the error tolerance is less than 10^{-3}.

The velocity profiles predicted by LBM and FLUENT at various cross-sections are shown in Figure 10. The solid lines denote the prediction obtained by LBM while the symbols denote the predictions obtained by FLUENT. The velocity profiles at all cross-section predicted by LBM agree very well with those predicted by FLUENT, as shown in Figure 10a. The development length for velocity field at *Re* = 800 in this flow is expected to be x/H= 47.4. The thermal filed has the same development length as the hydrodynamic field since *Pr* is selected to be unity. The nearly fully-developed velocity profile obtained by both method at $X = 0.725$ also agree very well with each other. They also agree well with the analytical solution, $U = 6\,(Y–Y^2)$, for the fully developed laminar velocity profile, as shown in Figure 10b.

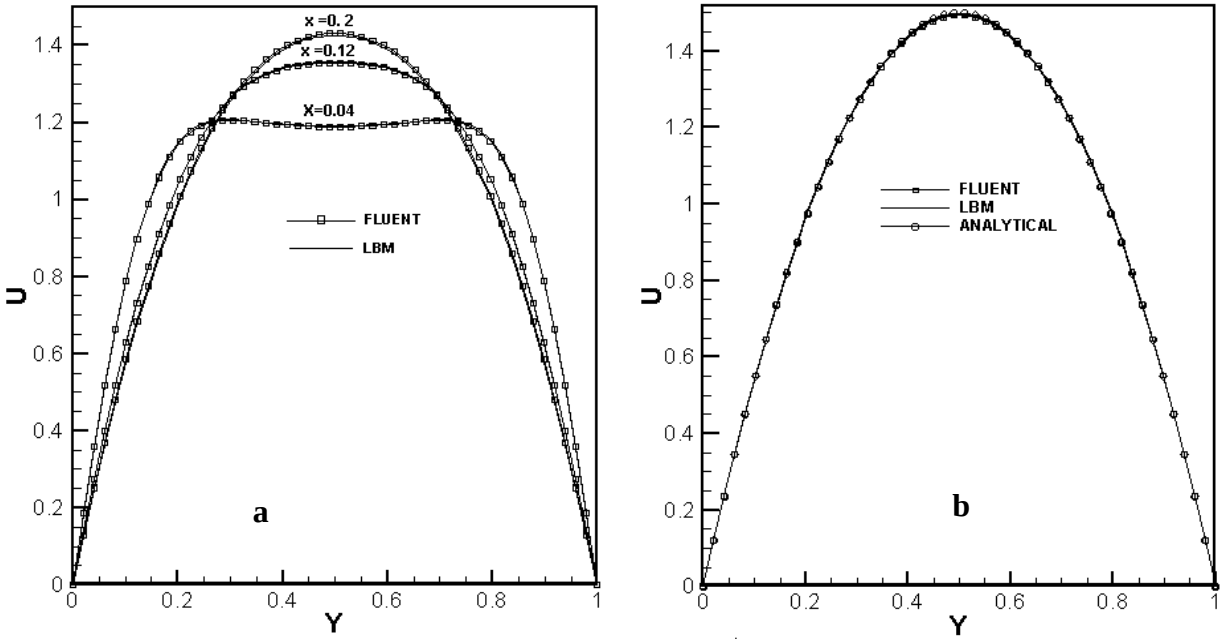

Figure 10. a) Velocity profiles at various cross sections predicted by LBM and FLUENT b) Velocity profile at X = 0.725 predicted by LBM and FLUENT and the self-similar velocity profile of the fully developed flow

The temperature profiles predicted by LBM and FLUENT at various cross-sections are shown in Figure 11. The solid lines denote the prediction obtained by LBM and the symbols denote the predictions obtained by FLUENT. The temperature profiles predicted by LBM agree very well with those predicted by FLUENT.

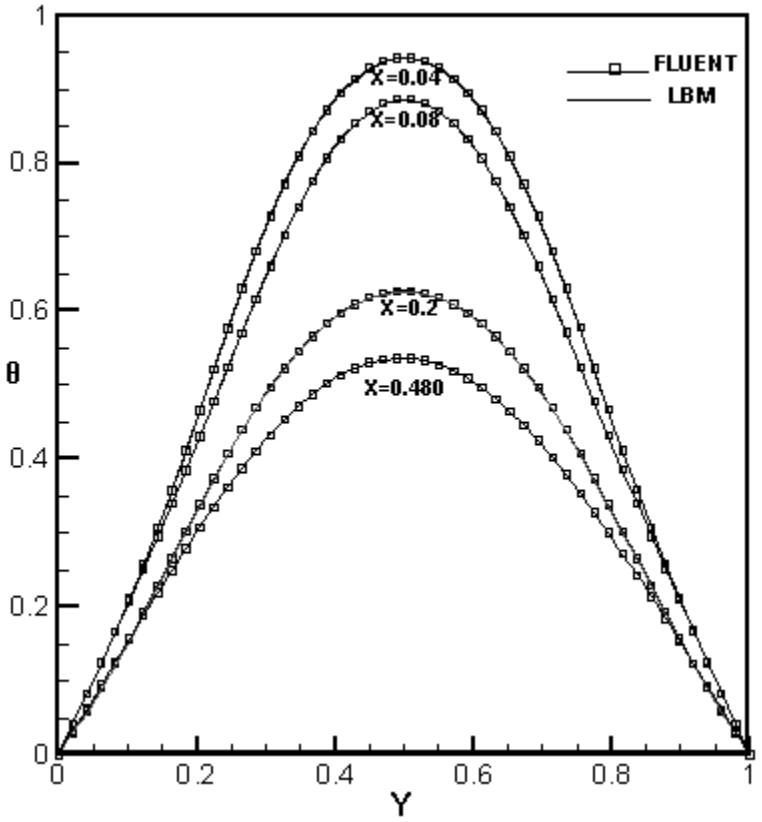

Figure 11. Temperature profile at various cross-sections predicted by LBM and FLUENT.

Wall shear stress and heat transfer coefficient are predicted at various cross sections in the developing region. The local value of skin friction, C_f, and the Nusselt number, Nu, are determined

$$C_f(X) = \frac{\mu}{{}^1\!/_2 \rho U_{in}^2} \frac{\partial u}{\partial y}(x,0) = \frac{4}{Re}\frac{\partial U}{\partial Y}(X,0) \quad and \quad Nu(X) = 2\frac{T_{in}-T_w}{T_m-T_w}\frac{\partial \theta}{\partial Y}(X,0) \qquad (2.52)$$

where T_m is the bulk temperature of the fluid and is calculated at each cross-section as

$$T_m = \frac{1}{\int UdA} \int [T_w + (T_{in}(0.5H) - T_w)\theta]\, Ud \qquad (2.53)$$

The skin friction and the Nusselt number predicted by LBM are plotted in Figure 7 as a function *x*/2*H*. ReC_f tends to 24 as the fully developed region is approached. Similarly, Nusselt number tends to 7.54 as the thermally fully developed region is approached, as shown in Figure 7b. These values are in perfect agreement with the fully developed values of C_f and *Nu* as well documented in the literature.

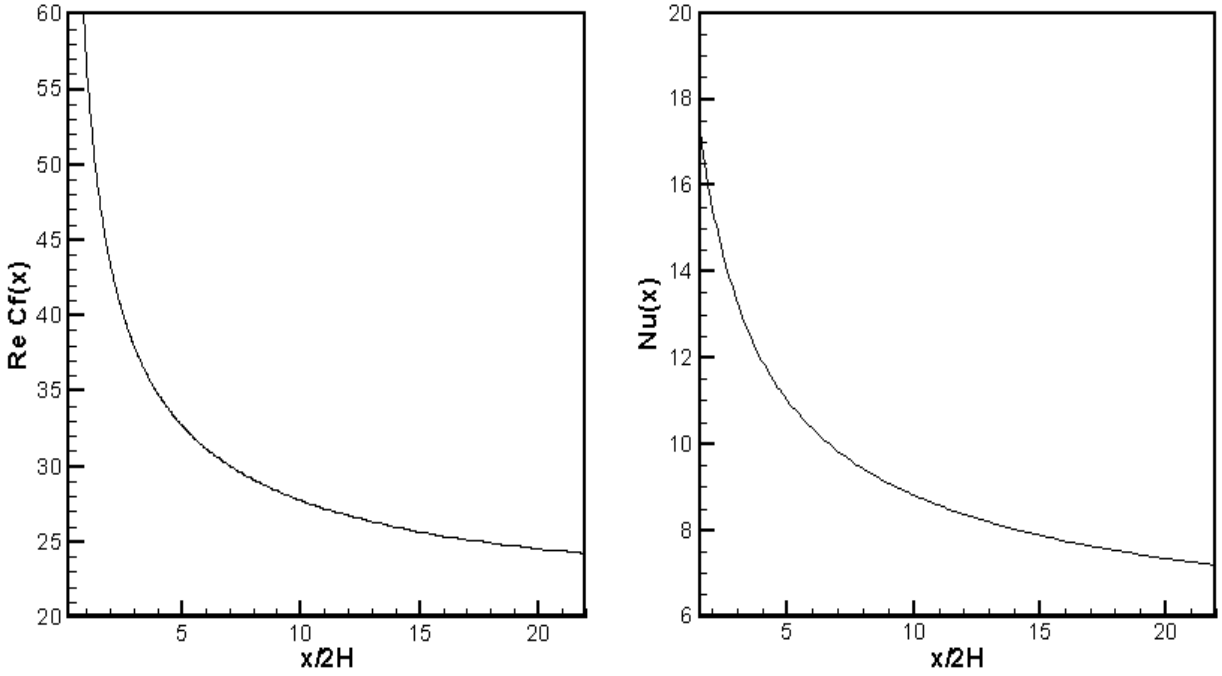

Figure 12. a) Skin friction and b) Nusselt number plotted as a function of *x*/2*H*.

Consequently, hydrodynamically and thermally developing laminar steady flow in a channel is considered as an example to illustrate that Lattice Boltzmann method is a promising computational fluid dynamics tool. D2Q9 lattice arrangement is used to predict both velocity and temperature field. Profiles obtained by LBM-D2Q9 and ANSYS-

FLUENT agree very well. Away from the inlet as the fully developed region is approached and the profiles tend to self-similar solutions of fully developed flows. That is confirmed by prediction of the skin friction and Nusselts number. They tend to well-known fully developed values as full developed region is approached away from the inlet.

CHAPTER 4: NON-ISOTHERMAL TWO DIMENSIONAL LID- DRIVEN FLOW

Thermal lattice Boltzmann method is applied to investigate lid-driven cavity flow at various Reynolds number. The range of Reynolds number considered here is Re=1000 to 10000. The velocity and temperature fields predicted by LBM at various Reynolds are compared against those predicted by ANSYS-FLUENT and those documented in the literature [1,2]. Objective of this study is solving complex flow problems and show that LBM can be an effective CFD tool.

4.1 PROBLEM STATEMENT

Non isothermal lid-driven cavity flow is considered for various Reynolds number. The aspect ratio is taken AR=L/H=1. The upper boundary is moving with a constant speed while others boundaries are stationary. The boundary conditions imposed on the velocity and temperature field is shown in the figure below. The temperature of the moving boundary is at 100^{o}C while others boundaries are kept at 50 ^{o}C.

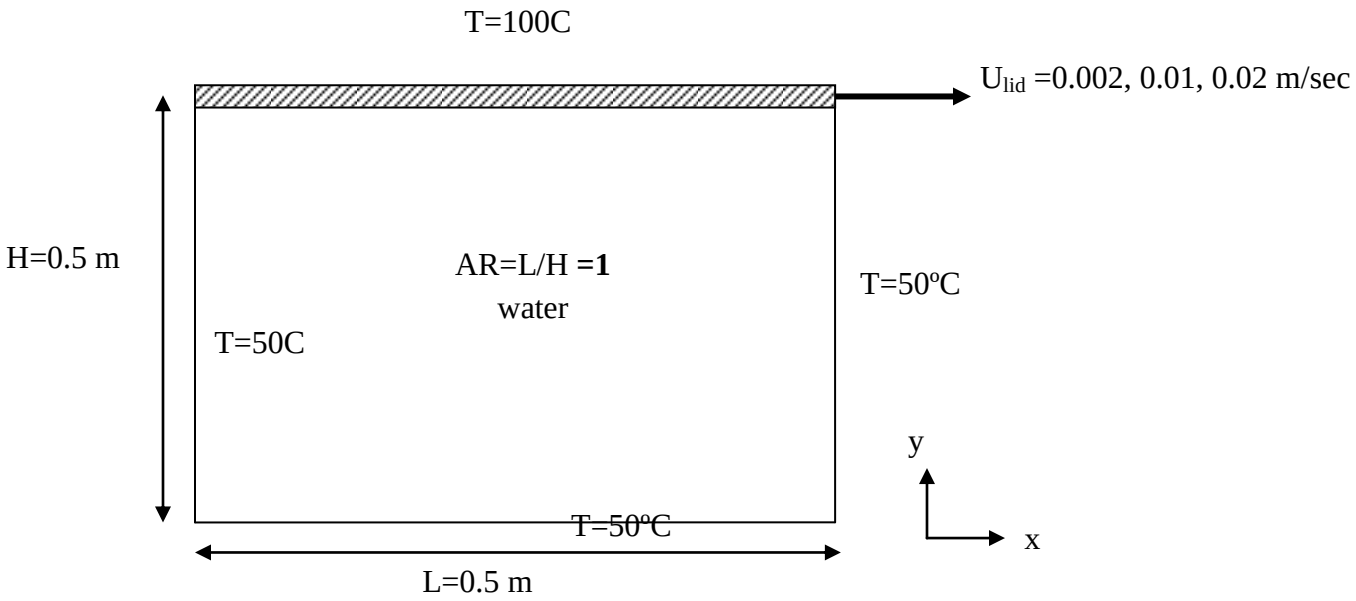

Figure13. The geometry of flow domain

4.2. APPLYING LATTICE BOLTZMANN (D2Q9) TO HEATED LID DRIVEN CAVITY

4.2.1. Normalized Parameters

The advantage of scaling parameters is to reduce the number of variables pertaining to the physical situation but it still describes the behavior of solution. The velocity and temperature field predicted by both LBM and ANSYS-FLUENT for Re=1000, Re=5000, and Re=10000.

The scaling parameters are

$$\theta = \frac{T - T_w}{T_{lid} - T_w}, \qquad \theta(\mathrm{X}=0) = 0, \quad \theta(\mathrm{X}=1) = 0, \ \mathrm{Re} = \frac{\mathrm{u}_{\mathrm{lid}} H}{\upsilon}$$

$$\theta(\mathrm{Y}=0) = 0, \quad \theta(\mathrm{Y}=1) = 1\ , \quad X = \frac{x}{L}, Y = \frac{y}{H}, \ \mathrm{U}_{\mathrm{lattice}} = \upsilon_{lu}\ \frac{\mathrm{Re}}{M}$$

$$0 \le X \le 1, 0 \le Y \le 1, \ \mathrm{u}_{\mathrm{nd}} = \frac{\mathrm{u}}{\mathrm{U}_{\mathrm{lattice}}}, \nu_{nd} = \frac{\nu}{\mathrm{U}_{\mathrm{lattice}}}$$

The flow domain and the boundary conditions are displayed in Figure 14 in terms of normalized variables.

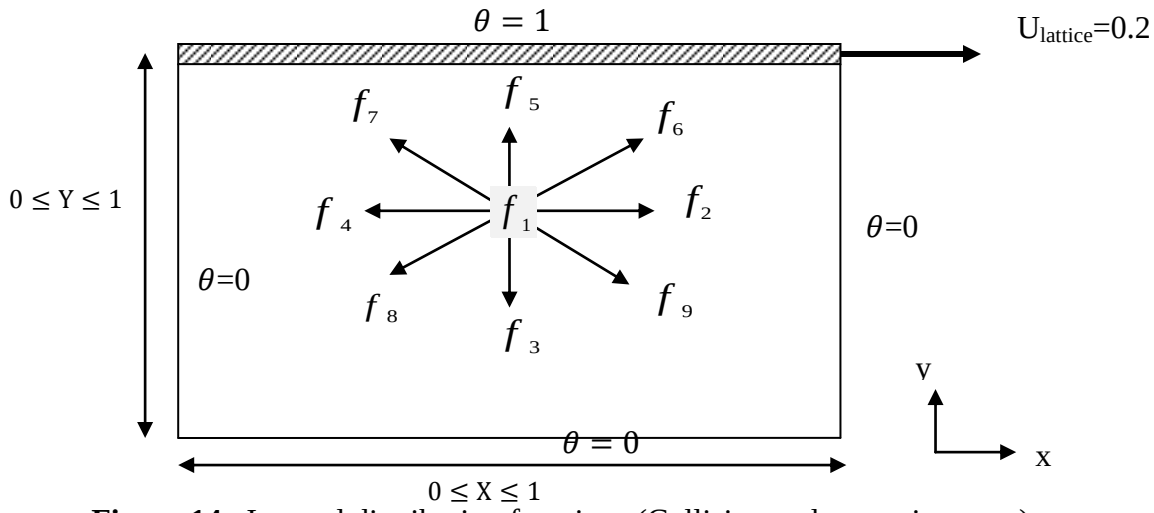

Figure 14. Internal distribution functions (Collision and streaming term)

The velocity per unit lattice is defined using the velocity of the lid. The macroscopic Reynolds number is equal to the lattice Reynolds number. Applying the conservation of mass and momentum at the moving boundary condition yields

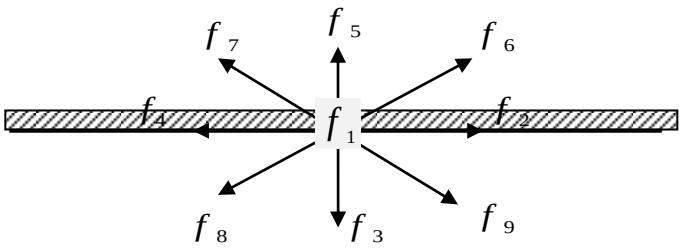

Figure 15a. Distribution functions at the upper boundary

Distribution functions f_3 , f_8 and f_9 at the upper boundary are unknown and expressed by

$$\rho_u = f_1 + f_2 + f_4 + 2\times(f_5 + f_7 + f_6) \tag{2.54}$$

$$f_3 = f_5 \tag{2.55}$$

$$f_8 = f_6 + \frac{1}{2}(f_2 - f_4) - \frac{1}{2}\rho_u \times u_{lid} \tag{2.56}$$

$$f_9 = f_7 + \frac{1}{2}(f_4 - f_2) + \frac{1}{2}\rho_u \times u_{lid} \tag{2.57}$$

The second order bounce back type boundary condition for the velocity field is used at other three boundaries. Typical distribution functions at these boundaries are displayed in Figure 15b.

At the left Boundary, the unknown distribution functions f_2, f_6 and f_9 are determined by

$$f_2 = f_4 \tag{2.58}$$

$$f_6 = f_8 - \frac{1}{2}(f_2 - f_4) \tag{2.59}$$

$$f_9 = f_7 + \frac{1}{2}(f_4 - f_2) \tag{2.60}$$

At the right boundary, the unknown distribution functions f_4, f_7 and f_8 are determined by

$$f_4 = f_2 \tag{2.61}$$

$$f_8 = f_6 + \frac{1}{2}(f_4 - f_2) \tag{2.62}$$

$$f_7 = f_9 - \frac{1}{2}(f_4 - f_2) \tag{2.63}$$

For lower boundary condition, the unknown distribution functions are f_5, f_6 and f_7

$$f_5 = f_3 \tag{2.64}$$

$$f_6 = f_8 - \frac{1}{2}(f_4 - f_2) \tag{2.65}$$

$$f_7 = f_9 - \frac{1}{2}(f_4 - f_2) \tag{2.66}$$

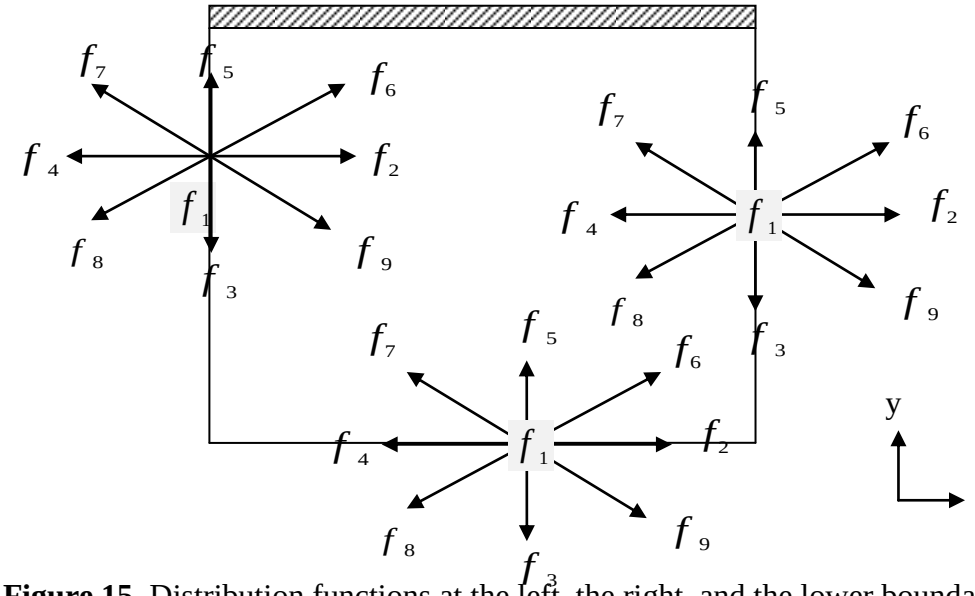

Figure 15. Distribution functions at the left, the right, and the lower boundary

4.3. Results and Discussion

The velocity and temperature field are presented in this section for at various values of Reynolds numbers. The results predicted by LBM are compared against those documented by Ghia et [10] and E.Elruck et [11] and are also compared against results obtained by ANSYS-FLUENT.

4.3.1. Velocity, &Temperature For Re=1000

Velocity profiles in transversal and the flow directions are plotted at various cross-section and compared against with those obtained by FLUENT, and those documented in the literature. The x-component velocity obtained by using LBM at X=0.5 is plotted as function of Yin Figures16 and 17. The x-component of the velocity predicted by Fluent and documented by Ghia et al (1982) is also plotted in Figures 16 and 17. The square line denotes the result obtained by FLUENT while the delta line denotes the results obtained by LBM. The circle line denotes the results obtained by Ghia et in 1982.

As clearly seen from Figures 16 and 17 the velocity profiles obtained by LBM &Fluent and documented in the literature agree very well.The x and y components of the velocity at various X and Y locations are also displayed in Table 1.1.

Table 1.1. Normalized horizontal and transversal velocity values at various grid points

Grids location	u/Ulid			v/Ulid		
	0.25	0.5	0.375	0.25	0.5	0.375
0	0	0	0	0	0	0
0.003333	-0.00075	-0.01253	0.004079	-0.00075	-0.01255	0.004079
0.179982	-0.22664	-0.3921	-0.23631	-0.22664	-0.39245	-0.23631
0.183315	-0.22991	-0.3915	-0.24341	-0.22991	-0.39185	-0.24341
0.839916	0.200663	0.335378	0.230551	0.200663	0.335581	0.230551
1	1	1	1	0	0	0

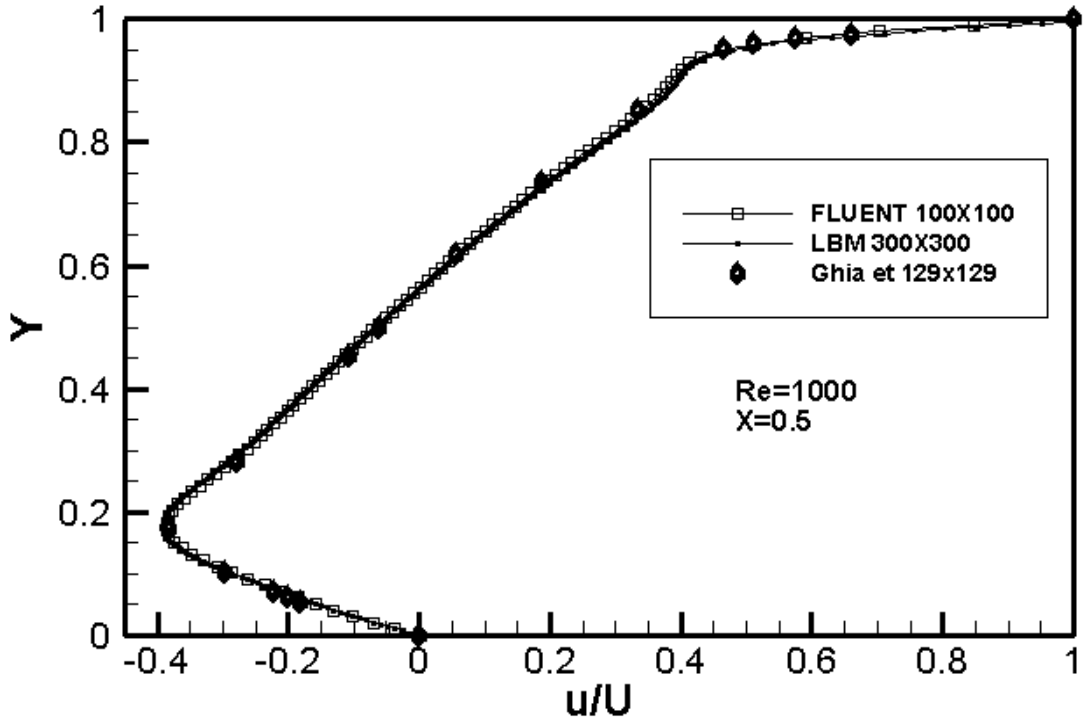

Figure 16. Normalized horizontal velocity at X=0.25 of Re=1000 for uniform grids for each method

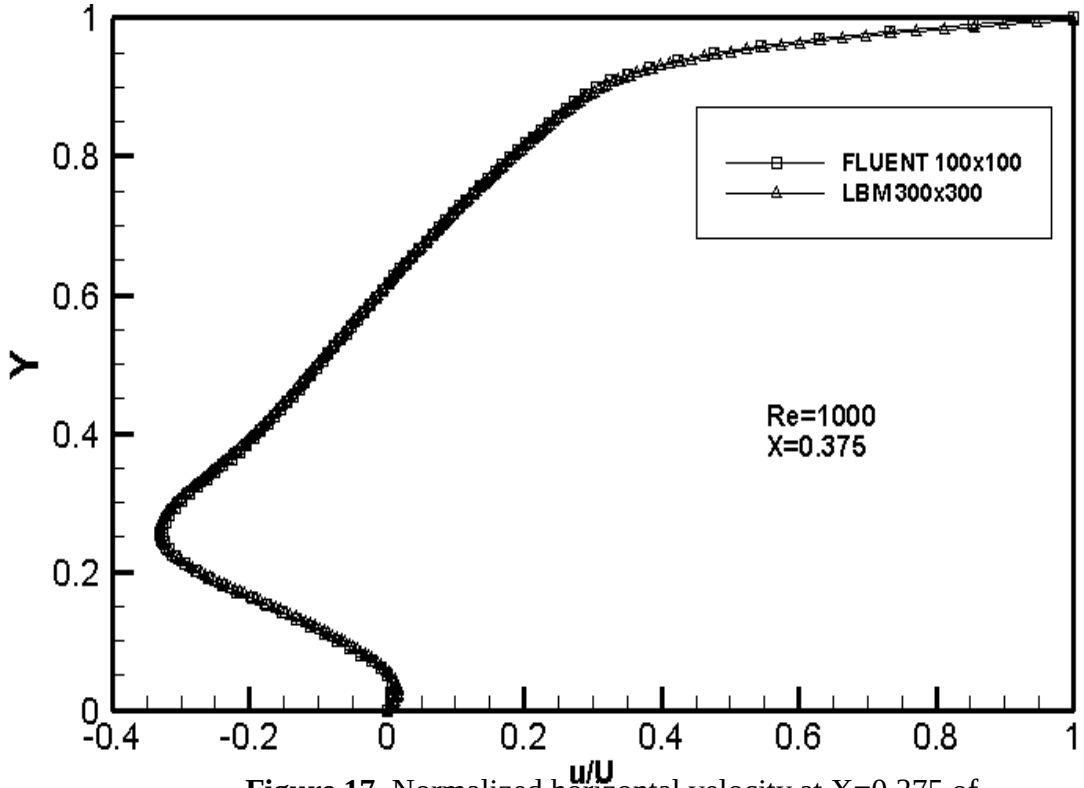

Figure 17. Normalized horizontal velocity at X=0.375 of Re=1000 for uniform grids for each method

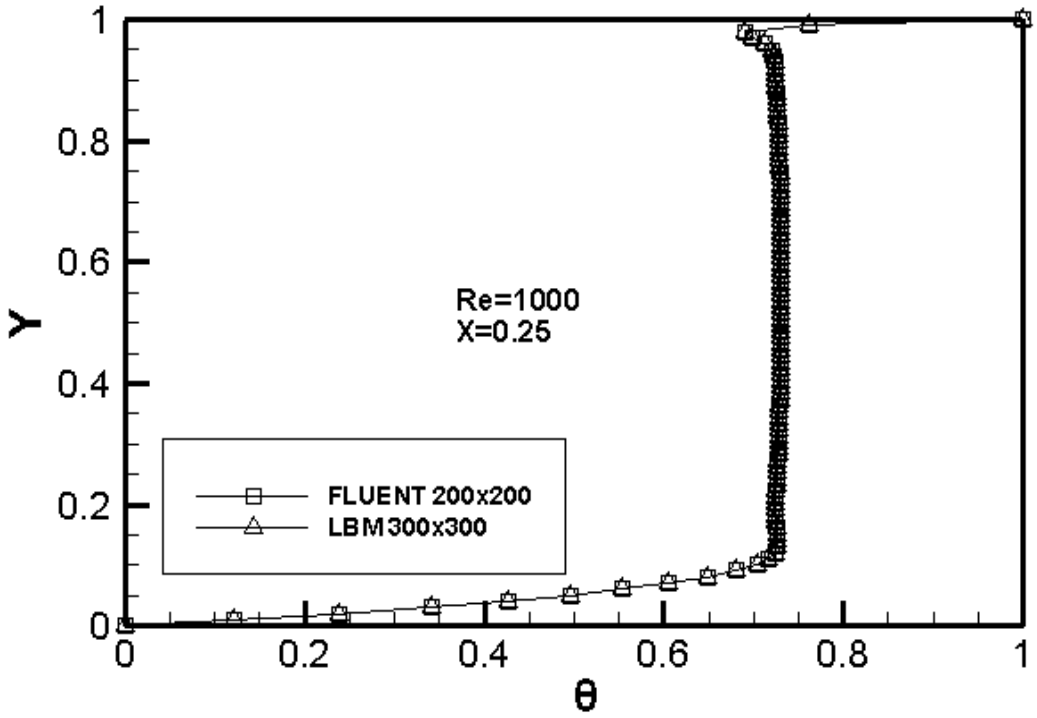

Figure 18. Normalized temperature at X=0.25 of Re=1000 for uniform grids for each method

Figure 18 displays temperature profiles predicted by LBM and FLUENT at X=0.25 for Re=1000, and Pr=7.01. The square line denotes the temperature profile obtained by FLUENT while the delta line denotes the temperature profile obtained by LBM. Both temperature profiles agree very well.

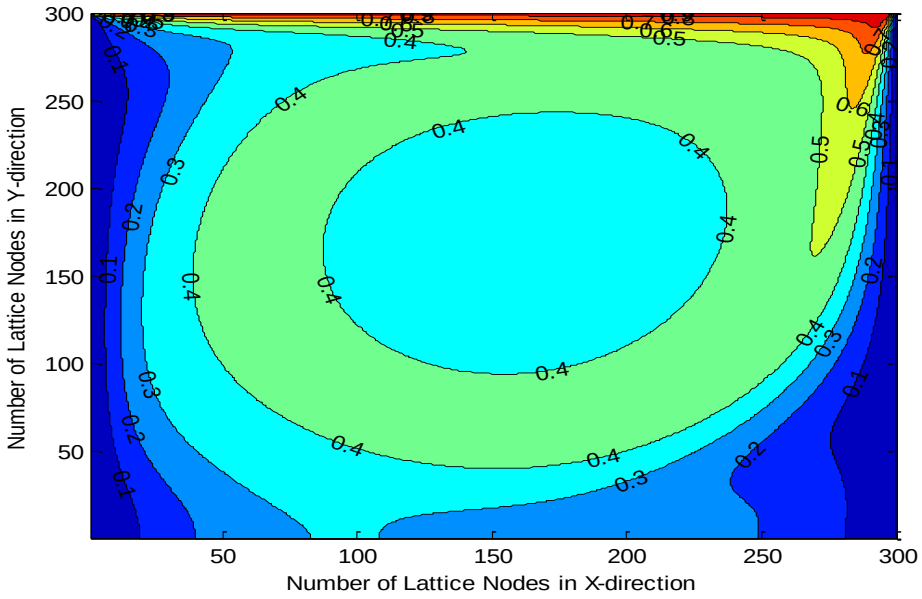

Figure19. Temperature contour of Re=1000 for uniform Grid 300x300 using LBM

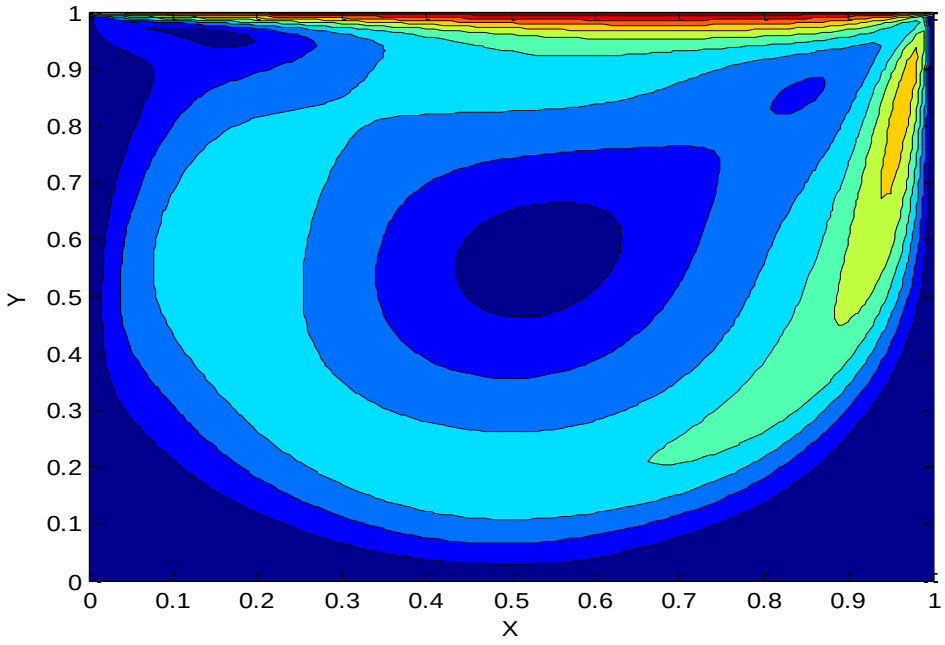

Figure20. Velocity contour of Re=1000 for Uniform Grid 300x300 using LBM

Figure19 shows the contour of isotherms predicted by thermal LBM. Fluid near the upper boundary is warmer compared to that of near lower boundary since the lid is heated while

the other boundaries are kept at lower temperature. Figure 20 displays the velocity contour predicted by LBM.

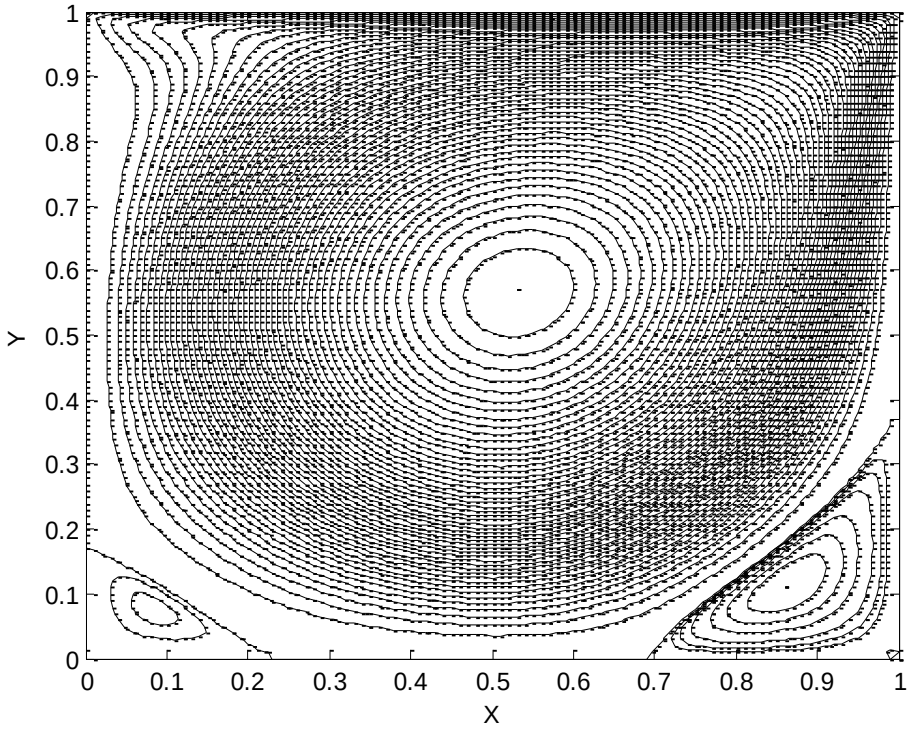

Figure21. Streamlines contour of Re=1000 for uniform grid 300x300 using LBM

Streamlines of the lid-driven cavity flow predicted by LBM for Re=100 is shown in Figure 21.A large size of corner eddy is present in right and left corners.. There is an onset small eddy at the top left corner. The streamlines predicted by LBM matches closely to that documented by Ghia et al [10] and by Erturk et al [11] . The 2nd order bounce back boundary condition for Re=1000 captures all eddies in thee lower corner of the square lid-driven. No eddies appear in the top right corner. As Re is increased the eddy that about the onset at Re=1000 in later subsection in this chapter becomes stronger and larger. The second order bounce back boundary condition has limitation to provide

an accurate solution. As it is observed here, it can be applied for Reynolds number up to 10000. For Re greater than 10000 more accurate discretization should be applied at the boundary.

4.3.2. Velocity and Temperature profiles at Re=5000

Normalized x-and y-component of the velocity predicted by LBM is listed in Table1.2. The x-component velocity obtained by LBM and Fluent are plotted as a function of Y at X=0.25 and X=0.5. The lines with square denote the profiles obtained by Fluent while the lines with triangle denote the profiles predicted by LBM. The velocity profiles predicted by both method at x locations agree very well, as shown in Figure 22 and 23.

Table 1.2. Normalized horizontal and transversal velocity values at various grid points

Grid location	u/Ulid			v/Ulid		
	0.25	0.5	0.375	0.25	0.5	0.375
0	0	0	0	0	0	0
0.010101	0.00543	-0.11143	0.055191	-9.77E-06	0.001425	-4.50E-05
0.060606	-0.09037	-0.38266	0.028156	0.00123	0.003974	0.000882
0.828284	0.257625	0.299918	0.225488	-0.00323	-0.00242	-0.00323
0.838384	0.263453	0.312698	0.237819	-0.00335	-0.00253	-0.00335
0.848486	0.268004	0.325789	0.250567	-0.00347	-0.00266	-0.00347
1	1	1	1	0	0	0

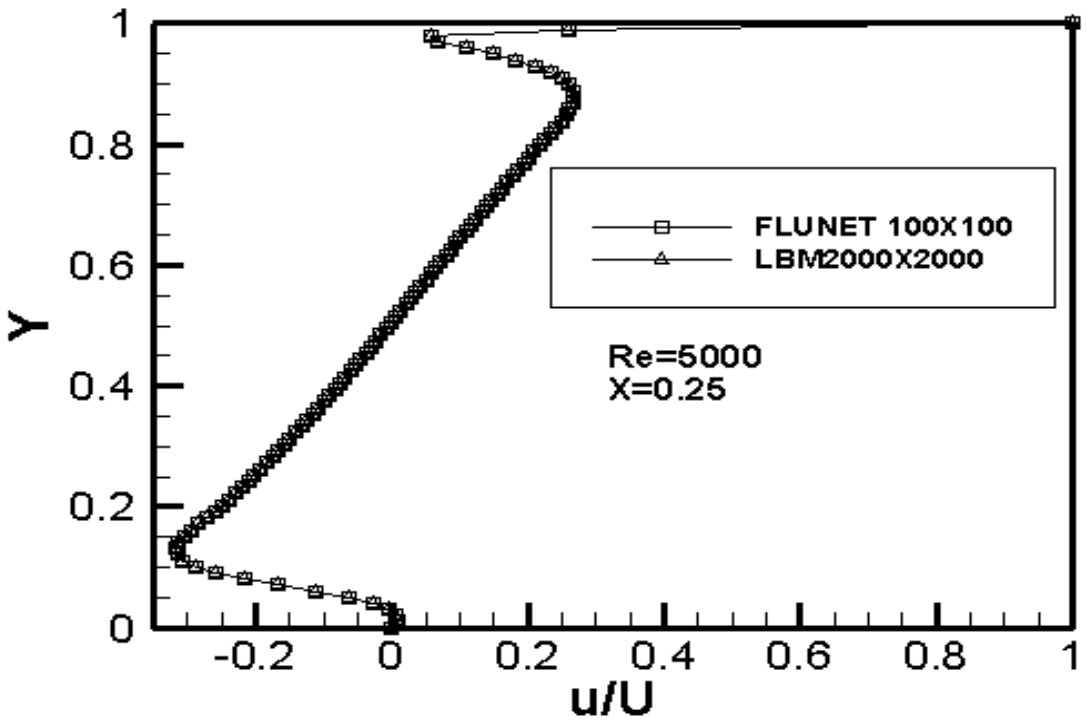

Figure 22. Normalized horizontal velocity at various cross-section of Re=5000 for uniform grids for each method

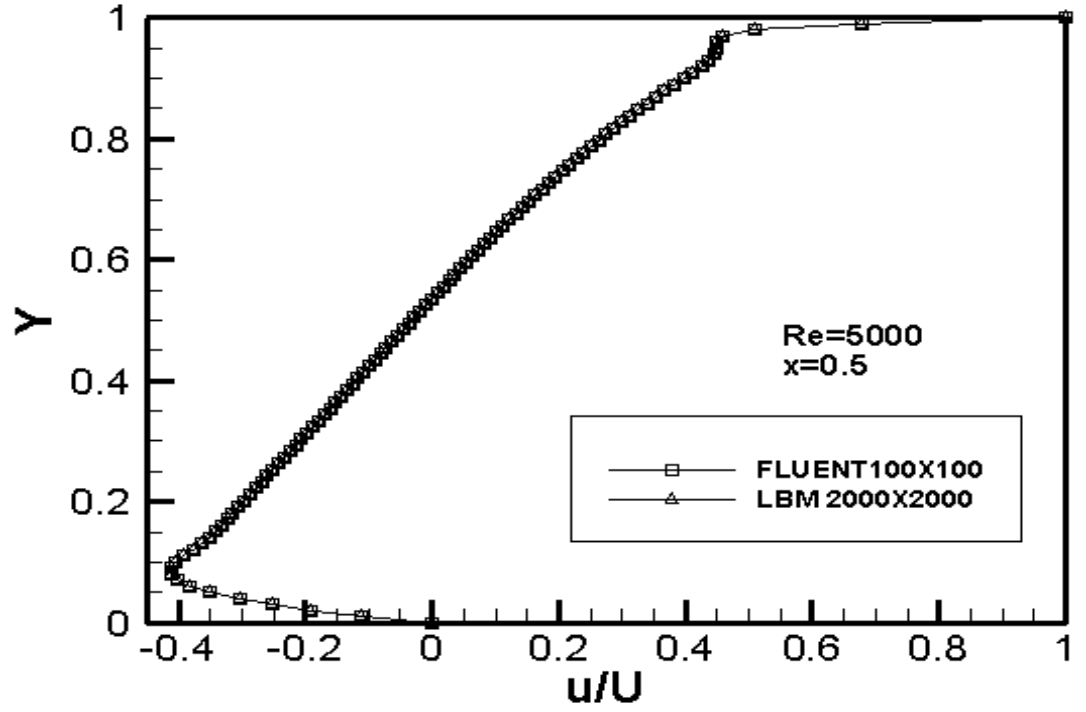

Figure 23. Normalized horizontal velocity at various cross-section of Re=5000 for uniform grids for each method

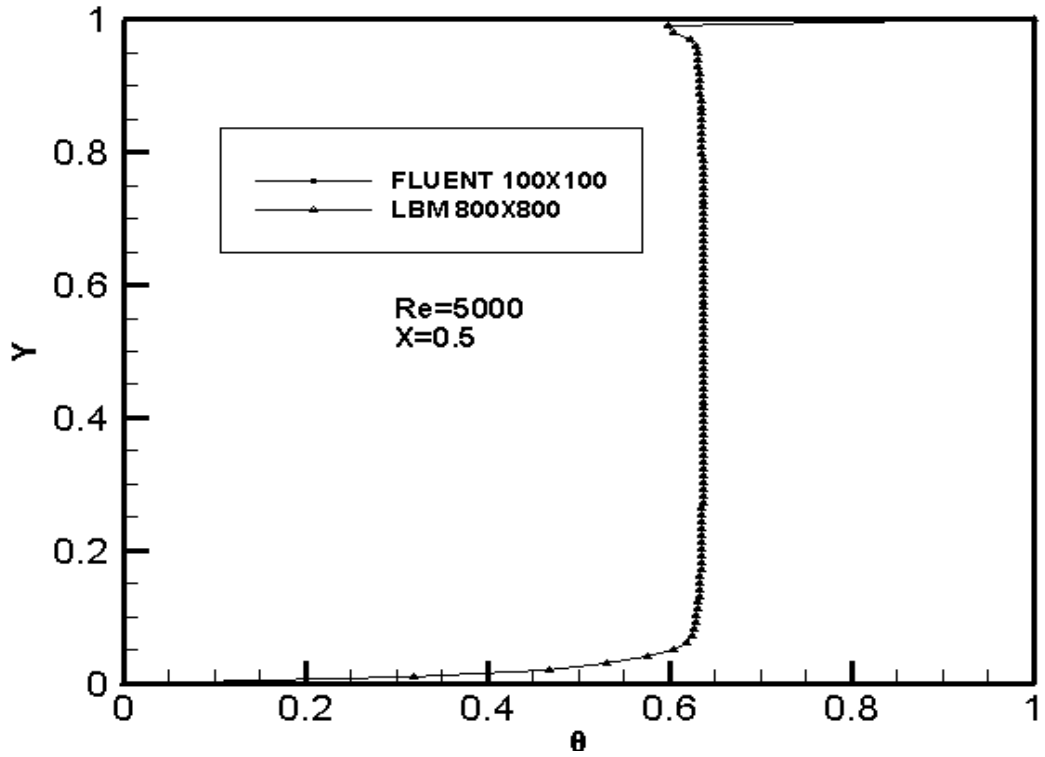

Figure 24. Normalized temperature at X=0.5 of Re=5000 for uniform grids for each method

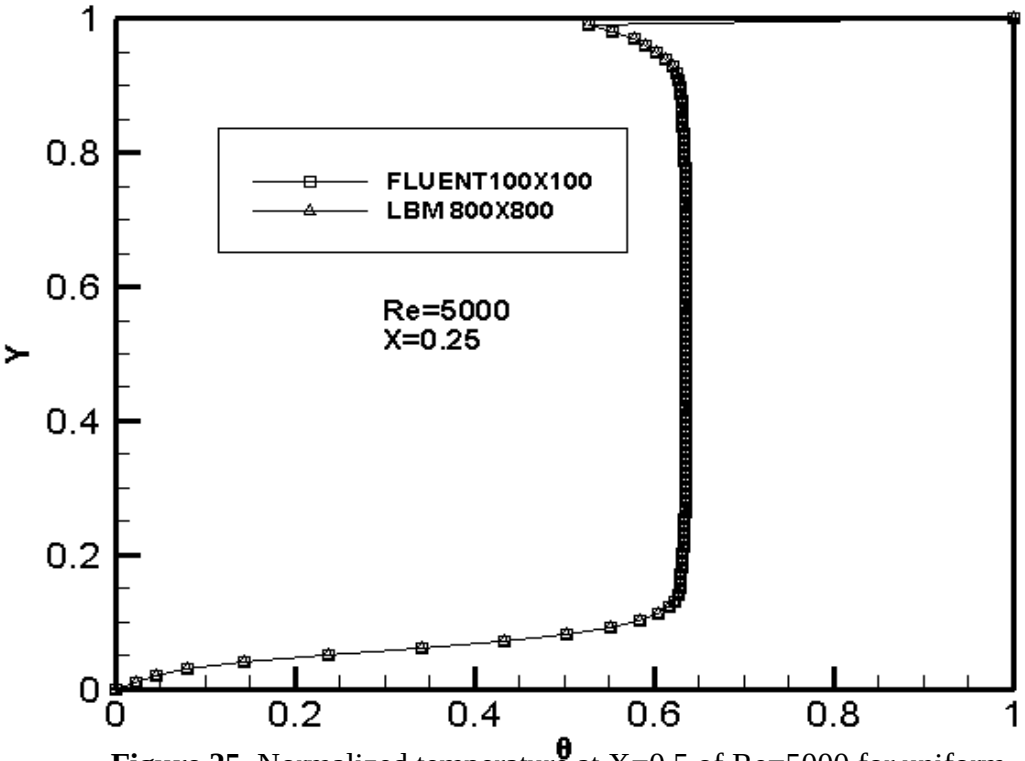

Figure 25. Normalized temperature at X=0.5 of Re=5000 for uniform grids for each method

In the previous Figures 24 and 25, they display the temperature profiles predicted by LBM and Fluent at X=0.5 and X=0.25 plotted against Y. The temperature is normalized to be 0 and 1, with (θ=1) represents the temperature of the moving boundary and (θ=0) represents the temperature of the stationary boundaries

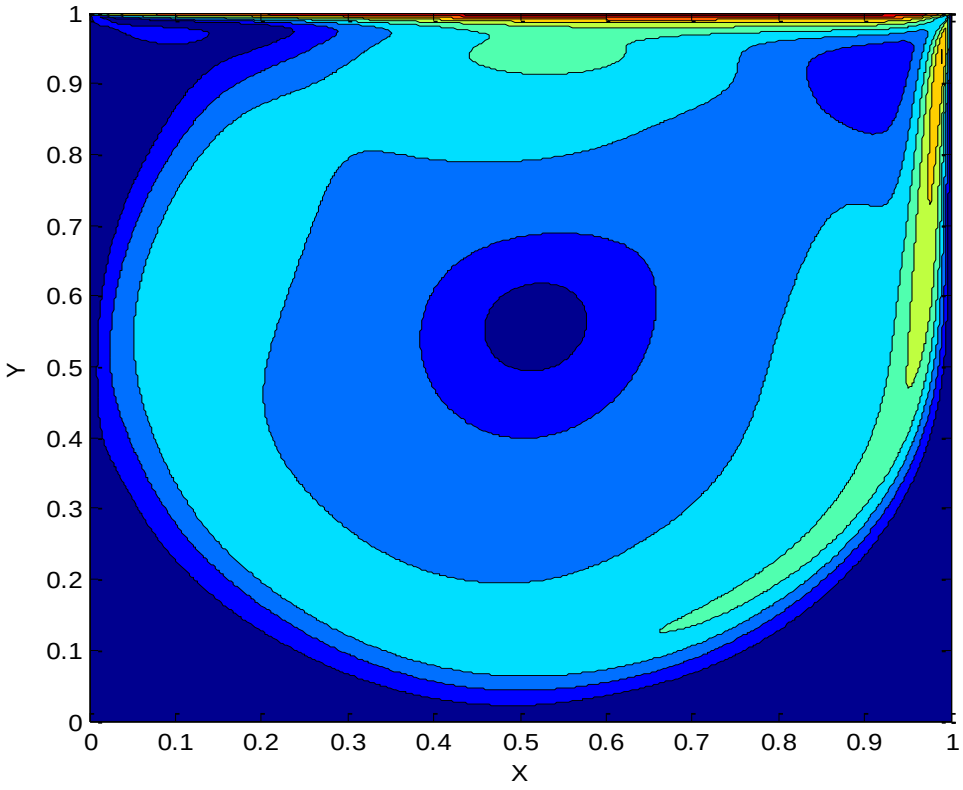

Figure26. Velocity contour of Re=5000 for uniform Grid 800x800 using LBM

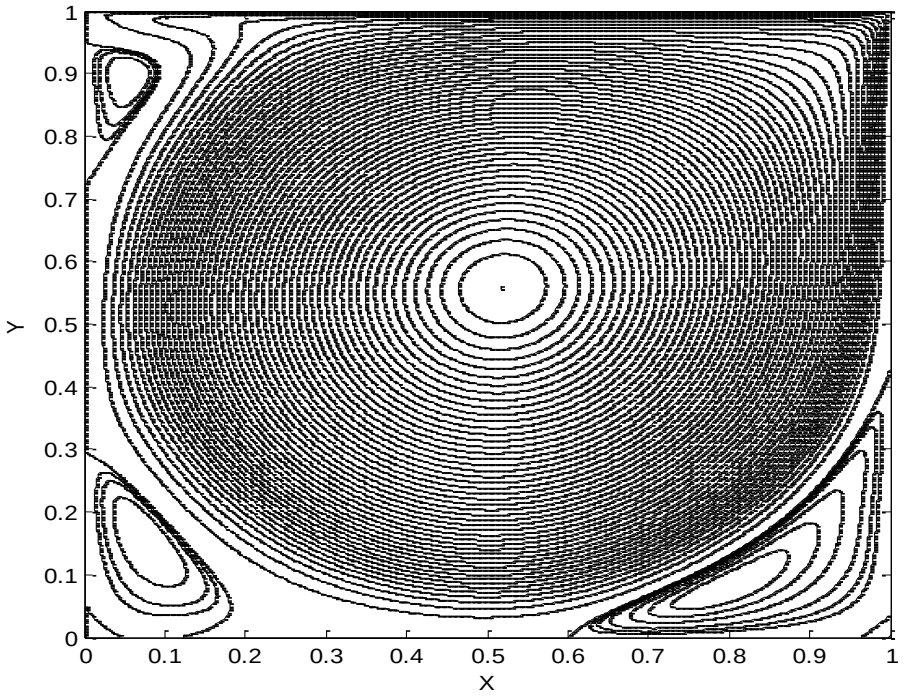

Figure27. Streamlines of Re=5000 for uniform Grid 800x800 using LBM

Figures 26 and 27 depict the velocity contour and streamlines, respectively. There are two large eddies at the bottom corners and the eddy at top left corner becomes larger at this Re. The streamlines predicted by LBM agrees well with streamlines documented by Ghia et al[10] and Ertruck et al [11] for Re=5000.

4.3.3. Velocity and Temperature profiles at Re=10000

Normalized x-and y-component of the velocity predicted by LBM is listed in Table1.3. The x-component velocity obtained by LBM and Fluent are plotted as a function of Y at X=0.25 and X=0.5. The lines with square denote the profiles obtained by Fluent while the lines with triangle denote the profiles predicted by LBM. The velocity profiles predicted by both methods at x locations agree very well, as shown in Figure 28 and 29.

Table 1.3. Normalized horizontal and transversal velocity values at various grid points

Grid location	u/Ulid			v/Ulid		
	0.25	0.5	0.375	0.25	0.5	0.375
0	0	0	0	0	0	0
0.010101	0.007782	-0.14762	0.063658	0.003309	-0.00034	-0.00018
0.060606	-0.11228	-0.38012	-0.0107	0.007891	0.002929	0.002179
0.828284	0.241463	0.261229	0.200086	-0.00562	-0.00657	-0.00419
0.848486	0.255871	0.285508	0.223652	-0.00585	-0.00676	-0.00441
1	1	1	1	0	0	0

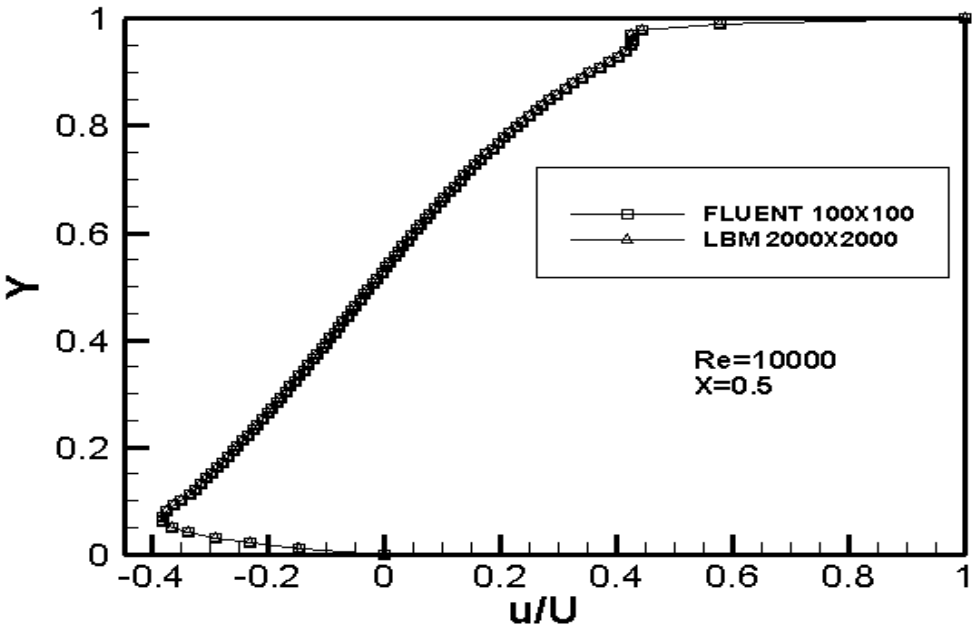

Figure 28. Normalized horizontal velocity at X=0.5 of Re=10000 for uniform grids for each method

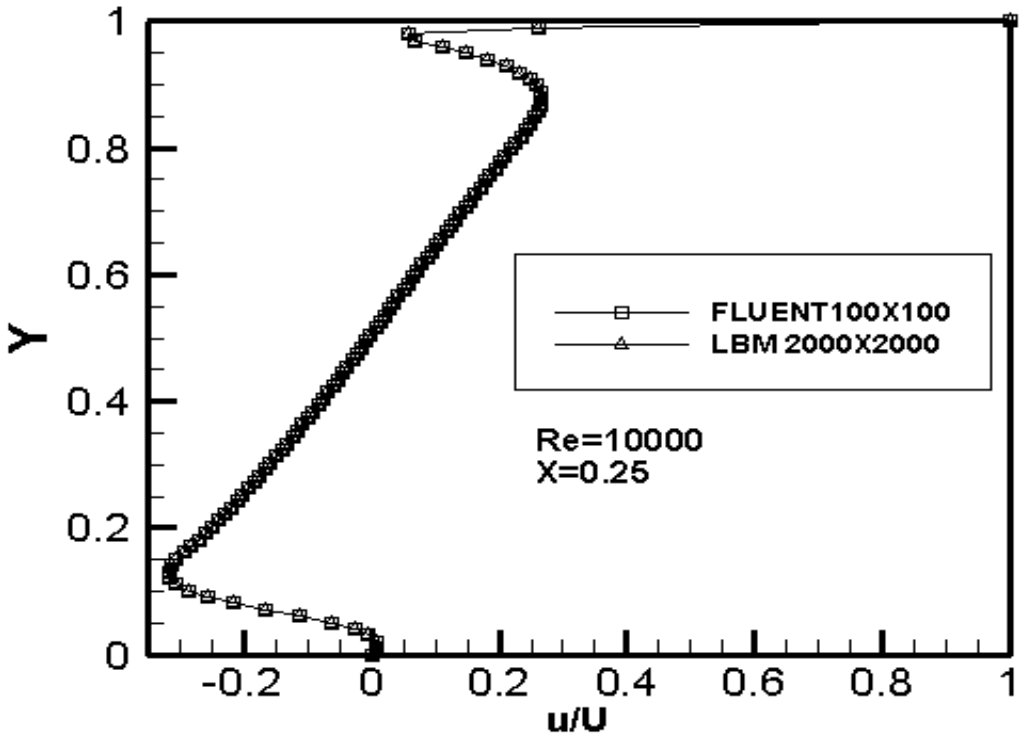

Figure 29. Normalized horizontal velocity at X=0.5 of Re=10000 for uniform grids for each method

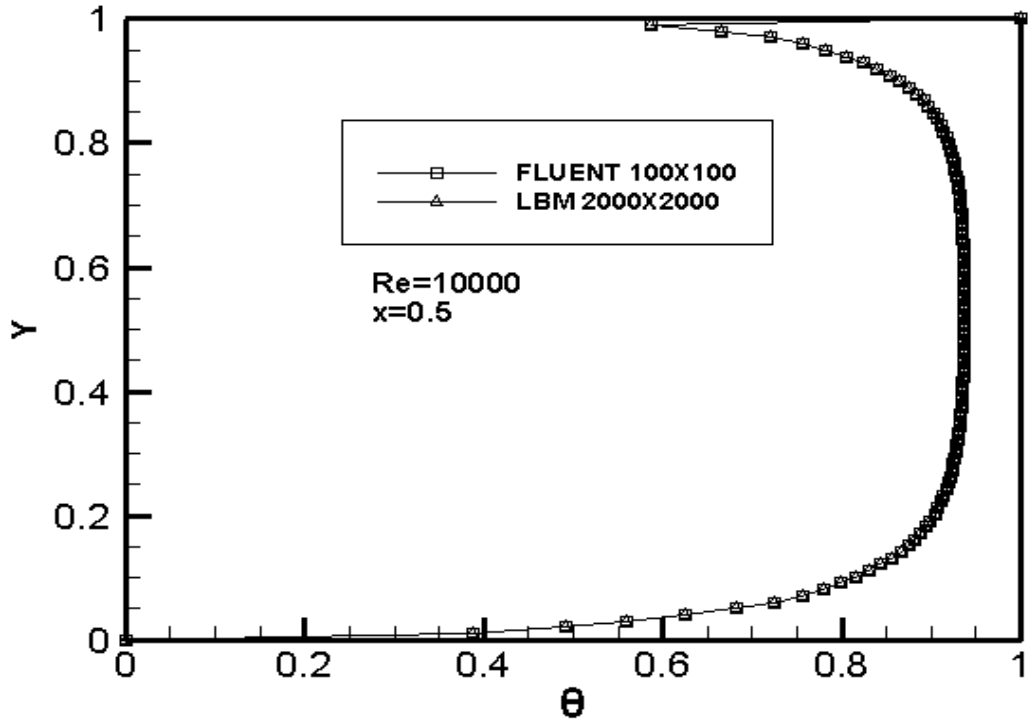

Figure 30. Normalized temperature at X=0.5 of Re=10000 for uniform grids for each method

In the separated the Figures 28 and 29, the square line represents the results obtained by FLUENT while the delta line represents the results obtained by LBM.

In the separated plots in the Figure 30, the temperature profiles are plotted at X=0.5 against those obtained by FLUENT. The temperature is normalized and the lid temperature is (θ=1) and the wall temperatures are (θ=0). The velocity profiles are shown in the figure 26 at various cross-sections, the boundary layer in the wall of the lid-driven cavity strongly affects on the velocity profiles.

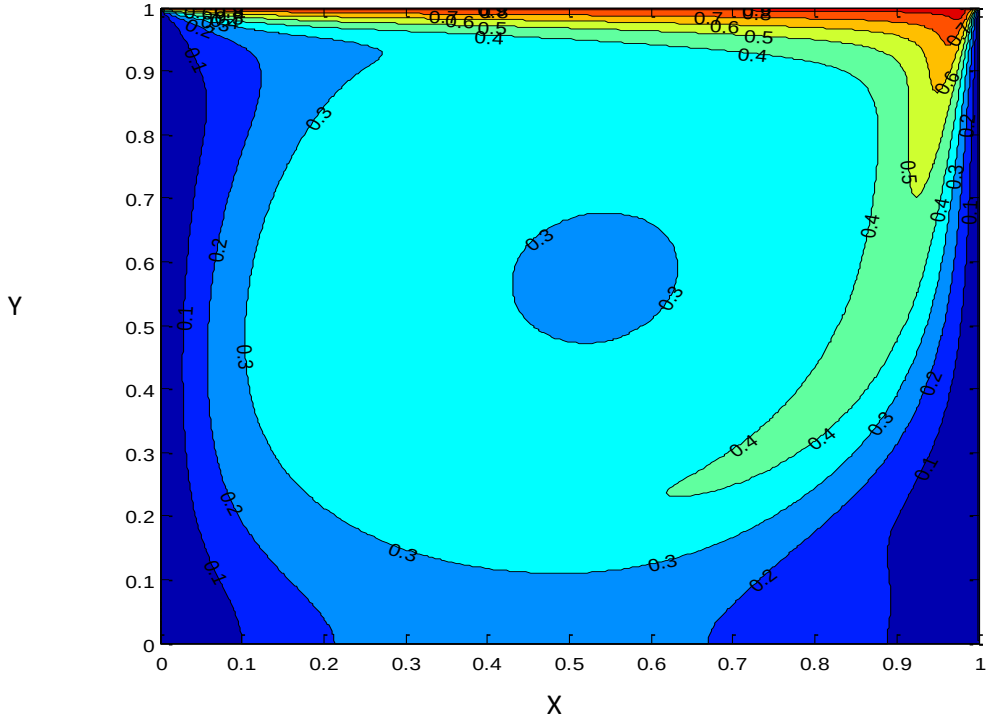

Figure31. Temperature contour of Re=10000 for uniform grid 2000x2000

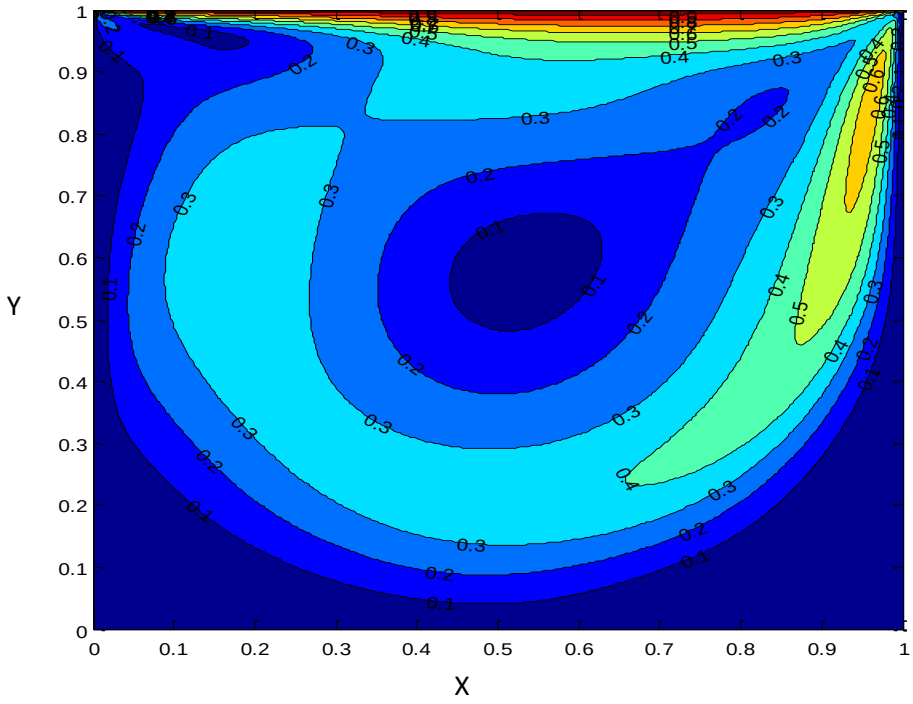

Figure 32. Velocity contour of Re=10000 for uniform grid 2000x2000

In the Figure31 , the temperature contour plotted for the whole flow cavity domain which shows that the higher temperature at the upper of the cavity (lid region) and the temperature varies since the temperature of cavity wall is placed at cold temperature (θ=0). The velocity contour represents the resultant velocity in x-direction and y-direction as shown in the Figure32. The temperature contour behaves similar to the velocity contour. The lid is heated at normalized temperature θ=1 and the others walls are placed at cold temperature which is normalized by θ=0.

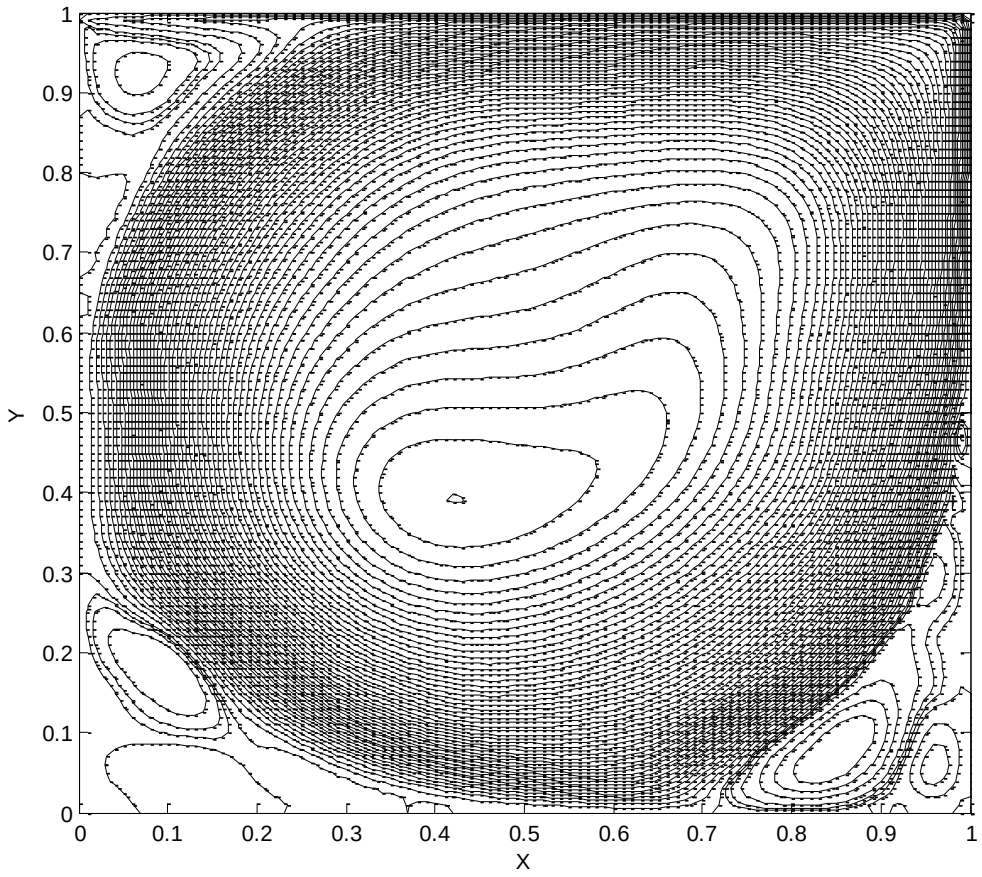

Figure33. Streamlines contour of Re=10000 for uniform grid 2000x2000 using LBM

The figure 33 displays the streamlines predicted by LBM for Re=10000. The bottom right corner region of the flow structure becomes very complicated with the presence of small and large scale eddies. This result implies that the second order bounce back type of boundary condition is not accurate enough to capture the flow structure at this high Reynolds number.

CHPATER 5: CONCLUSION & FUTURE WORK

5.1. CONCLUSION

Two dimensional nine directional (D2Q9) thermal lattice Boltzmann method has been developed to investigate nonisothermal flow problems. Velocity and temperature field of hydrodynamically and thermally developing flows in the entrance region of a channel has been predicted by the lattice Boltzmann technique. The velocity and temperature profiles at various cross sections in the developing region have been compared against those predicted by the ANSYS-Fluent. The profiles obtained by both methods agree very well. The nonisothermal lid-driven cavity flow at various values of Reynolds number up to 10,000 has also been considered to validate the thermal lattice Boltzmann method as an effective computational fluid dynamics tool. The velocity and temperature profiles obtained using both thermal LBM and Fluent are compared for Re = 100, 1000 and 10000. The profiles predicted by both methods at all Re agree very well and they also agree well with results documented earlier by previous investigators. Strong agreement between the results obtained by LBM and Fluent for both problems proves that the thermal lattice Boltzmann technique can be used to investigate complex flow and heat transfer problems. The author is currently investigating the possibility of using the LBM method developed here for multi-phase complex flow problems and phase change problems.

5.2. FUTURE WORK

LBM method is proven to be a promising CFD tool. The author will develop the thermal lattice Boltzman method to investigate transient multiphase flows of solids, liquids and gasses in two or three dimensional systems. Developing of LBM method to investigate

three dimensional unsteady complex multi-phase flows is underway. Transient three dimensional multiphase flows pose a challenge for traditional CFD tools. The setup of LBM suits well to handle the transient multiphase flows.

REFRENCES

[1] Qisu Zou and Xiaoyi He. On pressure and velocity flow boundary conditions and bounceback for lattice Boltzmann BGK model. PACS numbers:471.45-x;47.60.+1. arXiv:comp-gas; 21Nov 1996.

[2] Renwei Mei, Lattice Boltzmann Method for 3-D Flows with Curved Boundary. NASA/CR-2002-211657 , June 2002.

[3] G. McNamara and G.Zaneti,Phys. Rev.Lett.61,2332,1988.

[4] Sauro Succi. The Lattice Boltzmann Equation for Fluid Dynamics and Beyond. Published in USA by Oxford University Press Inc.,NY;2001.

[5] A. J. C. Ladd1 and R. Verberg. Lattice-Boltzmann Simulations of Particle-Fluid Suspensions. Journal of Statistical Physics, Vol. 104, Nos. 5/6, September 2001

[6] Raoyang Zhang and Hudong Chen. A Lattice Boltzmann method for simulations of liquid-vapor thermal flows. rXiv:physics/0210054v1; 11 Oct 2002

[7] Burce J. Palmer and David R.Rector. Lattice Boltzmann Algorithm for Simulating Thermal Flow in Compressible Fluids. Journal of Computational Physics 161,1-20; 9 March 1999

[8] X.D. Niu, C.Shu, Y.T Chew. A thermal lattice Boltzmann model with diffuse scattering boundary condition for micro thermal flows. Science Direct computers &fluids;2006.

[9] Jinku Wang, A lattice Boltzmann algorithm for fluid–solid conjugate heat transfer, Scince and Direct;March 2007.

[10] U. GHIA, K.N. GHIA, C.T.SHIN, High-Re Solutions For Incompressible Flow Using the Navier-Stokes Equations and a Multi-grid Method, Academic press, Inc; 9182

[11] E. Erturk, T.C. Corke et. Numerical Solutions of 2D Steady Incompressible Driven Cavity Flow at High Reynolds Numbers, GYTE-BAP; 2003.

[12] Shiyi Chen and Daniel Martı´nez. On boundary conditions in lattice Boltzmann methods. American Institute of Physics, 20 May 1996

[13] Romana Begum, M. Abdul Basit. Lattice Boltzmann Method and its Applications to Fluid Flow Problems. EuroJournals Publishing, Inc. 2008

[14] Michael C. Sukop, Daniel T. Thorne,Jr. Lattice Boltzmann Modeling An introduction for Geosceintific and Engineers. Springer –Verlag Berlin Heidelberg USA;2010

[15] A. J. C. Ladd1 and R. Verberg. Lattice-Boltzmann Simulations of Particle-Fluid Suspensions. Journal of Statistical Physics, Vol. 104, Nos. 5/6, September 2001

[16] M. Sbragaglia, S. Succi. Analytical calculation of slip flow in lattice Boltzmann models with kinetic boundary conditions. Physics of Fluids; 12 September 2005

[17] Quan Liao and Tien-Chien Jen. Application of Lattice Boltzmann Method in Fluid Heat transfer,2001

[18] S. J. Almalowi, A. Oztekin, Flow Simulations using Two Dimensional Thermal Lattice Boltzmann Method, Journal of Applied Mathematics;2012.

VITA

NAME: Saeed J. Almalowi

ADDRESS: Lehigh University-Mechanical Engineering and Mechanics

27 Memorial Drive West, Bethlehem, PA 18015 USA. Tel. (610) 758-3000

E-MAIL: sja210@lehigh.edu

EDUCATION: B.Cs-King Abdul-Aziz University –KSA-2006

M.Cs: Lehigh University – PA 18015 USA-2012